03

Focusing diffraction optics for orbital telescopes

© V.V. Lider

Shubnikov Institute of Crystallography „Crystallography and Photonics“, Russian Academy of Sciences,
117333 Moscow, Russia

e-mail: vallider@yandex.ru

Received November 8, 2021
Revised March 1, 2022
Accepted March 18, 2022

The review is devoted to the principles, state of the art and problems of diffractive optics used to focus X-ray and γ-radiation in telescopes at orbital stations. Various multilayer structures for normal incidence telescopes, supermirrors for Wolter optics, Laue lens as a soft γ-radiation concentrator, as well as modified Fresnel zone plates for focusing radiation in a wide energy range with an unprecedented high angular resolution ($10^{-1}-10^{-3}{}''$).

Keywords: X-ray and γ-radiation, X-ray and γ-telescopes, diffraction, multilayer structures, Laue lens, Fresnel zone plates.

DOI: 10.21883/EOS.2022.07.54725.44-22

1. Introduction

Electromagnetic radiation is the primary source of data on celestial bodies. This radiation utilized by orbital telescopes may be divided tentatively into several bands: extreme ultraviolet (EUV) radiation with photon energy $E = 10-12\,\text{eV}$ (these energy values correspond to wavelengths of $10-120\,\text{nm}$), soft (SXR) with $E = 0.12-10\,\text{keV}$ and hard (HXR, $E = 10-100\,\text{keV}$) X-ray bands, and gamma radiation ($E > 100\,\text{keV}$).

Orbital observatories survey the hot matter of the Universe: gas heated to a temperature of $10^7-10^8\,\text{K}$ in the process of accretion of matter in close binary stars or active galactic nuclei, gas in galaxy clusters, and hot atmospheres of single neutron stars. The mechanism of generation of radiation with $E < 10\,\text{keV}$ in these sources is thermal in nature.

A number of astrophysical objects produce electromagnetic radiation with its properties being essentially independent of the temperature of the medium within which it is generated. It is commonly referred to as nonthermal radiation. The lack of dependence on the ambient temperature for nonthermal radiation with $E > 10\,\text{keV}$ is attributableto the fact that its energy is sourced not from the thermal energy of the medium, but from a small-size population of high-energy particles. Nonthermal X-ray radiation may be produced by radio pulsars, shock waves in supernova remnants, relativistic jets from active galactic nuclei and quasars, hot coronae of accretion disks in close binary stars, solar flares, etc. X-ray pulsars (accreting neutron stars with a strong magnetic field) are of special interest in this regard.

The basic technique of X-ray astronomy (and, for that matter, astronomy in general) is imaging of a specific region of the celestial sphere for subsequent examination of radiation sources. In the case of soft X-ray radiation, this task is performed with the use of grazing incidence optics (specifically, Wolter mirrors [1]). This method allows for an exceptional angular resolution ($< 1''$) and provides a relatively high effective data collection area (owing to the use of a large number of interleaved mirror shells). The field of view of such instruments is limited by the radiation grazing angle and is on the order of one degree.

Various wavelengths of EUV radiation, which is associated with solar regions characterized by specific values of temperature, plasma density, and magnetic intensity, are the primary sources of data on solar processes and activity. However, images acquired with the use of grazing incidence optics have a low or moderate spectral resolution and are not suitable for isolating a specific temperature or resolving macroscopic dynamic effects.

Single crystals are commonly used to isolate a narrow spectral transmission band in the HXR region. Their operation is based on constructive interference of waves reflected off crystal planes (the Bragg reflection process). In the EUV band, interplanar distances d of most crystals used in practice are too small to adhere to the constructive interference criterion set by the Bragg formula $2d\sin\theta = \lambda$ (λ is the radiation wavelength and θ is the Bragg angle). A stack of thin alternating material layers with its periodicity (d-interval) being equal to parameter d in the Bragg formula may be used to overcome this limitation.

Waves reflected off all boundaries of alternating material layers with a high contrast of optical indices interfere constructively, thus providing a high reflection coefficient and fine spectral selectivity [2]. A multilayer interference structure (MIS) prepared this way may be regarded as an artificial crystal that reflects radiation like natural crystals. These „synthetic“ multilayer systems have a tremendous advantage in that their layer thickness (and, consequently, periodicity) may be adjusted freely to match the wavelength that needs to be reflected at a specific angle [3].

Multilayer optics used in the geometry of normal incidence has an advantage over grazing incidence optics in enhanced efficiency and spatial resolution, relative ease

of manufacture and maintenance, and, consequently, in higher imaging quality. Multilayer normal incidence optics has fewer aberrations than grazing incidence optics, thus providing a higher angular resolution in a much wider field of view.

The use of grazing incidence geometry in high-energy ($E > 10$ keV) X-ray telescopes leads to a reduction in the spatial resolution and efficiency, since the grazing angle decreases rapidly with increasing energy, thus rendering the focal distance impracticably large and making the field of view (and the effective data collection area) too small. Bragg reflection off an MIS with its period varying smoothly with depth may be used to solve this problem and widen the transmission band [4].

Getting back to the subject of diffraction-based HXR and gamma optics, we note that both single-crystal lenses (e.g., Laue lens [5]) and Fresnel zone plates and their derivatives [6], which are distinguished by their high sensitivity and superior angular resolution, may be used in telescope systems.

The aim of this review is to introduce the reader to the field of focusing diffractive optics of orbital telescopes.

2. Focusing EUV radiation optics. Normal incidence telescopes

2.1. MIS for X-ray normal incidence telescopes

The issues of MIS physics and layer interfaces, the methods of deposition and diagnostics of such structures, and their applications have been discussed in detail in monographs [7,8] and reviews (e.g., [9–12]).

Featuring a combination of certain unique properties, MISs, which are occasionally referred to as multilayer mirrors, rank among the most versatile elements of current X-ray optics. The flexibility of MIS characteristics, the affordability and generality of their processing technology, and the feasibility of production of mirrors with high X-ray optical parameters boost the interest in their practical application as dispersive and reflective elements in X-ray astronomy.

A standing wave with amplitude B_m of modulation of the dielectric constant [13] forms as a result of interference of incident and reflected waves in an MIS (Fig. 1) consisting of alternating material layers with contrasting optical parameters (high-absorption scattering layers A and low-absorption spacer layers (spacers) B):

$$B_m = 2(\varepsilon_A - \varepsilon_B)\sin\pi m\gamma/\pi m\gamma. \quad (1)$$

Here, m is the order of reflection, $\gamma = d_A/(d_A + d_B) = d_A/d$, and d_A and d_B are the thicknesses of layers A and B, respectively. Permittivity ε is related to polarizability χ and refraction index n in the following way: $\varepsilon = 1 - \chi \approx n^2$; χ has real (Re) and imaginary (Im) parts ($\chi = \mathrm{Re}\chi + \mathrm{Im}\chi$), where the latter covers absorption in the medium. Thus, the reflection structure is modulated by function $\sin\pi m\gamma$;

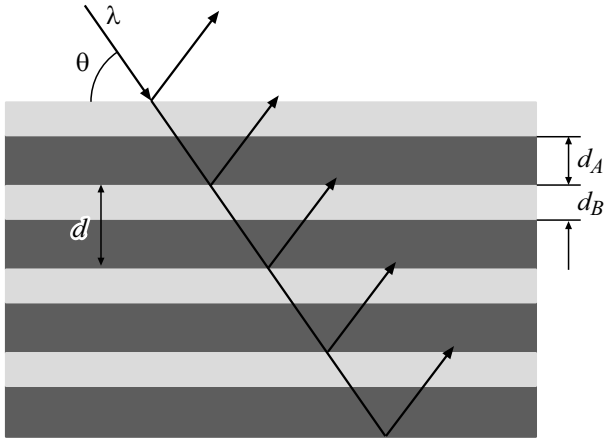

Figure 1. MIS structure. d_A and d_B are the thicknesses of absorber and spacer layers, d is the bilayer period, θ is the Bragg angle, and λ is the X-ray radiation wavelength.

i.e., factor γ specifies the relative peak reflectance and, specifically, suppresses diffraction peaks with $m = \gamma^{-1}$. For example, even Bragg peaks are suppressed at $\gamma = 0.5$, while odd peaks are amplified; multilayer structures with $\gamma = 0.5$ are called quarter-wave ones, since each layer covers exactly $\lambda/4$ of an incident wave.

Periodic X-ray MISs are commonly characterized by their reflection coefficient at the maximum of the diffraction reflection curve (R) and by the width of this curve ($\Delta\lambda$). The latter parameter specifies the width of the spectral transmission band ($\Delta\lambda/\lambda$) or reciprocal quantity $\lambda/\Delta\lambda$, which is referred to as the spectral resolving power. The transmission band is defined by number N of bilayers involved in the formation of a diffracted beam [14]:

$$\Delta\lambda/\lambda = 1/mN. \quad (2)$$

SXR and EUV regions present a unique challenge in that all usable materials are absorbing to a certain extent. This is the reason why quarter-wave MISs are rarely used as optical elements: the absorber thickness in quarter-wave structures is so large that the absorption often becomes too strong to achieve a high reflectance. Since the absorption of a thin and strongly absorbing material may be insignificant if it is located at the node of the standing-wave field, one needs to reduce the absorber thickness ($\gamma < 0.5$) to suppress the influence of absorption on the MIS reflectance. The optimum value of parameter γ^* is given by formula [8,13]

$$\mathrm{tg}\, t(\pi\gamma^*) = \pi[\gamma^* + \mathrm{Im}\,\chi_B/\mathrm{Im}\Delta\chi]. \quad (3)$$

The maximum reflectance $R_{\max}$ at $m = 1$ is then given by

$$R_{\max} = (1 - w)/(1 + w),$$
$$w = [(1 - C^2\cos^2\pi\gamma^*)/(1 + C^2\cos^2\pi\gamma^*(\mathrm{Re}\Delta\chi/\mathrm{Im}\Delta\chi)^2]^{1/2}, \quad (4)$$

where $\Delta\chi = (\chi_A - \chi_B)$ and $C = 1$, $C = \cos^2\theta$ for $p(\pi)$ and $s(\sigma)$ polarizations, respectively.

Therefore, the maximum possible coefficient of reflection off an MIS is specified completely by two parameters: $\mathrm{Re}\Delta\chi/\mathrm{Im}\Delta\chi$ and $\mathrm{Im}\chi_B/\mathrm{Im}\Delta\chi$. The enhancement of reflectance achieved by choosing the optimum value of γ is the product of a compromise between the effects of constructive interference of waves, which are reflected successively off the interfaces, and absorption losses.

If absorption is minimized, the number of bilayers used (N_{ef}) and, consequently, the resolving power increase [8,14]:

$$\lambda/\Delta\lambda \approx (\pi/2)N_{\mathrm{ef}} = (\sin^2\theta/\mathrm{Im}\chi)\{(1-C^2y^2) \times [1+C^2y^2(\mathrm{Re}\Delta\chi/\mathrm{Im}\Delta\chi)^2]\}^{-1/2}, \qquad (5)$$

where $y = \sin(\pi\gamma)/\pi[\gamma + \mathrm{Im}\chi_B/\mathrm{Im}\Delta\chi]$, $\chi = \gamma\chi_A + (1-\gamma)\chi_B$.

The selection criteria for MIS materials may be narrowed down to just three rules [7,8,13]. 1. A material with the lowest possible absorption coefficient should be chosen for intermediate layers.

2. The strongly absorbing MIS component should be chosen so that relation $\mathrm{Re}\Delta\chi/\mathrm{Im}\Delta\chi$ is maximized.

3. One should make sure that the interface between the chosen materials is physically and chemically stable. The issue of compatibility of materials is one of the most important ones; ideally, they should not interact chemically and interdiffuse.

The following parameters of a two-component MIS are subject to optimization: layer material types A and B, their thicknesses, layer ordering (*ABAB* .. or *BABA* ..), overall number of bilayers N, and multilayer period d. In general, the optimization process utilizes a target (search) function that is specified by the design assignment. The selection of proper multilayer materials by optical constants and stability is the starting point of the design process. The optimization of individual structures is a complex problem that may be solved only with the use of various computer algorithms [15–17].

2.2. Selection of MIS materials

Spacer and reflective materials are normally selected by analyzing the absorption spectra of various materials. Such spectral features as absorption edges of elements corresponding to the ionization potentials of K, L, M, ... electron shells are of interest in this respect. The absorption of X-ray radiation by matter is related to the interaction of photons with electrons of inner shells of an atom. If the photon energy exceeds the electron–nucleus binding energy (excitation threshold), an electron may be removed from an atom. This leads to a sharp increase (jump) in the absorption of X-ray radiation. The wavelength corresponding to the excitation threshold energy is referred to as the absorption edge of a given element. Since the absorption coefficient at wavelengths lying slightly above the absorption edge of an element may be fairly low (Fig. 2), such an element is fit for use as a spacer.

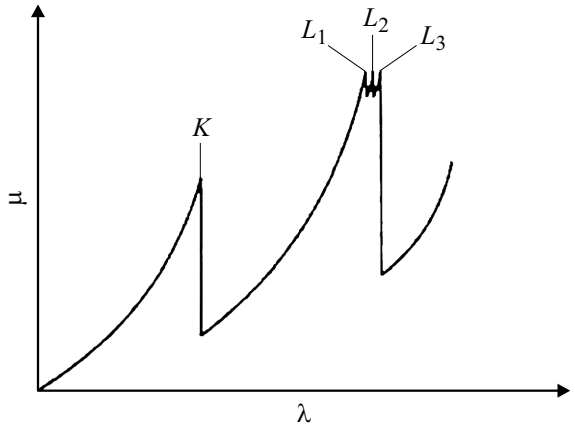

Figure 2. Schematic representation of absorption coefficient μ as a function of wavelength λ of the primary photon for three X-ray absorption edges (K, L_1, L_2, and L_3).

The diagnostics of solar corona plasma (with regard to temperature and density) is often hard to perform by imaging. The primary reason for this is that a multitude of spectral lines formed in different conditions fall within the telescope sensitivity range, which is specified primarily by the characteristics of mirrors in the optical system of a telescope. For example, lines of Fe X–XXIV ions excited in a wide temperature range from 1×10^6 to 16×10^6 K and several lines of other elements (O, Ca, Ni), which correspond to temperatures ranging from 0.3×10^6 to 5×10^6 K, are observed in the 17.7–20.7 nm wavelength region [18]. This makes it considerably more difficult to determine the temperature of observed plasma. Therefore, one needs to use an MIS with a narrow spectral transmission band that allows for observation of corona plasma at individual spectral lines.

The primary contribution to the spectral resolution of instruments is produced by the wavelength dependence of the reflection coefficient of reflective multilayer structures (MISs) in the optical system. Since the sensitivity of a telescope increases with increasing spectral selectivity $\lambda/\Delta\lambda$ of mirrors, the peak reflection coefficient is joined by the spectral selectivity, which depends on the type of materials used in X-ray MISs and the thickness ratio of materials within a single period (5), in the list of crucial characteristics of reflective coatings [19].

Range: 4.4–9.4 nm

In the wavelength range between the K absorption edges of carbon ($\lambda = 4.47$ nm) and boron ($\lambda = 6.63$ nm), one should use carbon, which is the most „transparent“ element in this region, as a light element of mirrors. Chromium is the optimum counterpart to carbon, since Cr/C-based MISs have been studied extensively at a wavelength of 4.47 nm. A Cr/C structure with period $d = 3.35$ nm and $\gamma = 0.35$ has the following calculated reflection characteristics: $R = 20.8\%$, $\lambda/\Delta\lambda = 118$ [19].

The authors of [20] have compared Mo/Y, Ru/B_4C, and Ru/Y MICS prototypes in detection of the Fe XVIII

solar line ($\lambda = 9.4$ nm). Mo/Y did indeed provide the highest reflection coefficient in this study ($R = 34\%$), while Ru/B_4C had a coefficient of 28.3% [21]. A Mo/Y MIS has been proposed for the first time in [22,23] and had a reflection index up to 46% at a wavelength of around 11.4 nm under almost normal incidence. At $\lambda \approx 9$ nm, the peak reflection coefficient of periodic narrow-band Pd/B_4C multilayer structures was considerably higher than the one of Mo/Y [24]. However, Pd/B_4C MISs are highly stressed, thus raising the risk of coating failure. Fine characteristics achieved in the studies of Mo/Y and Pd/B_4C motivated the development of a new system consisting of Pd and Y layers and thin (~ 0.6 nm) buffer B_4C layers deposited onto each interface for suppressing the interdiffusion of Pd and Y [25]. Periodic Pd/B_4C/Y multilayers achieve a peak reflection of 43% at $\lambda = 9.4$ nm [26].

At a wavelength of 6.7 nm, the reflectance is maximized if one uses multilayer mirrors with lanthanum reflectors and boron spacers. Boron is the spacer material of choice at this wavelength, since it is in immediate proximity to the K absorption edge of boron. Since pure boron is characterized by a very low magnetron sputtering rate, certain carbides, such as B_4C, are used in practice. The examination of La/B, La/B_4C multilayer mirrors revealed that La/B_4C multilayer structures have the best reflection coefficients [27].

Range: 13–35 nm

The 13–35 nm range of extreme ultraviolet wavelengths provides the greatest opportunities for examination of a wide spectrum of solar activity processes [28]. Bright lines of ions corresponding to the entire temperature range of solar plasma (from the upper chromosphere to the hottest corona structures) are found in this spectral region: Fe VIII, Fe XX, and Fe XXIII (near $\lambda = 13.1$ nm); Fe-IX ($\lambda = 17.1$ nm); Fe-XII ($\lambda = 19.5$ nm); Fe-XIV ($\lambda = 21.1$ nm); Fe-XV ($\lambda = 28.4$ nm); He-II ($\lambda = 30.4$ nm); and Fe-XVI ($\lambda = 33.5$ nm). Lines with different excitation temperatures are located fairly far from each other in the spectrum. Imaging the Sun in these channels and comparing the results, one may obtain data on the thermal structure of solar plasma.

Multilayer combinations of materials based on Si [29,30] are commonly used at wavelengths of 13–30 nm that exceed the wavelength of the L absorption edge of Si ($\lambda = 12.4$ nm). The current record reflectance of a well-studied Mo/Si [31–34] MIS at an SXR wavelength of 13.4 nm is 71% [32,33], which makes this optical arrangement the most sought-after for solar spectroscopy.

However, the reflection coefficient of Mo/Si decreases gradually with increasing wavelength. At a wavelength of 30.4 nm, the reflection coefficient drops approximately to 20%. Therefore, other multilayer mirrors with a high reflection coefficient should be used at this wavelength. The reflectance efficiencies of certain combinations of materials based on Mg and Si (including SiC/Mg, B_4C/Mg, Mo/Si, B_4C/Si, SiC/Si, C/Si, and Sc/Si MISs) have been studied in [35] as part of research into the production of a multilayer for $\lambda = 30.4$ nm. It was demonstrated that the SiC/Mg combination features the maximum reflectance and the narrowest transmission band. This combination was then used in development of a highly reflective multilayer material for He-II radiation.

Multilayers based on Al ($\lambda_{L3} = 17.1$ nm) may be used to fabricate mirrors for the $\lambda = 17-21$ nm spectral range, since a considerable number of aluminum-based multilayer combinations exhibit a significant reflectance in this region [36]. Two Al-based multilayer structures have been examined: SiC/Al and Zr/Al [37–41]. Specifically, the results of measurements of reflection properties of the Al/Zr structure at a wavelength of 17.1 nm with $\gamma = 0.36$, $R = 56\%$, and $\lambda/\Delta\lambda = 28$ have been reported in [39]. Al/Zr multilayers feature very low film stress values and fine temporal stability: the reflectance of the prototype MIS remained almost unchanged after several years [26]. This prototype had fine optical characteristics and maintained structural stability up to 200°C; the latter property is considered to be very useful in practice. The amorphous Al–Zr alloy at the interfaces becomes polycrystalline at temperatures above 300°C. This is the probable reason behind the reflectance reduction [40].

It was demonstrated in [41] that Be may be used as an optically contrasting material together with Al in periodic multilayer mirrors at wavelengths around 17 nm. At the same time, since the absorption of both Be and Al is low, these materials are expected to produce a unique combination of reflection characteristics: a record-high peak reflectance coupled with spectral selectivity. A reflectance of 46% was obtained for the Be/Al structure. Following the introduction of 1 nm of Si on top of Be layers in each period, the reflectance increased to 61% under normal incidence. This increase is attributable to the smoothing of interfaces in Be/Si/Al multilayer mirrors: the RMS roughness in pure Be/Al structures is 1.3 nm, and the corresponding value in samples with a silicon spacer layer is 0.6 nm.

Owing to its optical constants, magnesium ($\lambda_{L3} = 25.1$ nm) is the most efficient material for spacer layers in the 25–35 nm wavelength range [42]. The He-II ($\lambda = 30.4$ nm) emission line, which was chosen for solar physics applications (e.g., solar corona imaging), necessitates the use of multilayer mirrors with a high reflectance. Several combinations of materials (including SiC/Mg, B_4C/Mg, C/Mg, Co/Mg, and Si/Mg [35,43]) have been examined for the design of mirrors operating at a wavelength of 30.4 nm. The reflectance values of Co/Mg and SiC/Mg MISs turned out to be the highest ones and reached 40.3% and 44.6%, respectively, under almost normal incidence. The obtained results demonstrate that SiC/Mg and Co/Mg multilayer mirrors hold promise for application at a wavelength of 30.4 nm.

SiC/Mg MISs attract research interest owing to a unique combination of high reflectance (more than 40% [44,45]), fine spectral selectivity, thermal stability (up to 350°C), and almost zero stress [45–48].

However, the SiC/Mg system is prone to catastrophic degradation due to Mg corrosion. This problem makes

Mg/SiC coatings ill-suited for applications that require long-term stability (e.g., for use aboard orbital telescopes [48]). The Si/B_4C/Mg/Cr multilayer structure turned out to be superior to other MISs in terms of reflection efficiency and long-term stability in the $\lambda = 30$ nm spectral range. B_4C and Cr layers prevented the interdiffusion of Si and Mg layers [49].

The substitution of magnesium with its compounds not prone to oxidation or interaction with other MIS materials appears to be beneficial. Magnesium silicide Mg_2Si was proposed in [39] to be used as a light mirror material in the 25–35 nm wavelength range. The Co/Mg system offers a higher thermal stability [50]. In addition, it was demonstrated [51] that interfaces in the Co/Mg system are sharp and Co and Mg layers do not interdiffuse. In view of this, it is important to choose a proper material counterpart to magnesium: this material should not interact with Mg and feature such optical characteristics that ensure a high reflection coefficient. Zirconium is an example of a material of this kind. Magnesium and zirconium do not interact with each other. The authors of [52] have demonstrated that the thermal stability of Zr/Mg mirrors annealed at temperatures up to 600°C is higher than the one of Y_2O_3/Mg, SiC/Mg, and Co/Mg mirrors. The reflectance of a Zr/Mg MIS is 30.6% at a wavelength of 30.4 nm. The reflection coefficient decreases slightly with increasing annealing temperature in the range up to 500°C and drops to 15.1% at 600°C. This degradation of characteristics is attributable to the interface roughness induced by stress relaxation.

The authors of [53] have reported the results of studies aimed at the development of optimized MISs for future narrow-band telescopes. Si/Mo, Si/Mo_2C, Si/B_4C, Si/C, and Si/SiC multilayers were compared. All these bilayers are designed for narrow-band imaging in the 25–35 nm wavelength range. It was found that Si/B_4C multilayers provide the highest reflection coefficient. Unfortunately, although the thermal stability of Si/B_4C is decent, adhesion turned out to be poor: cracking was observed in all the studied samples after 10 months of storage in air. This poor adhesion is likely attributable to high film stress values; if stress is indeed the culprit, it should be possible to enhance adhesion in future studies by revising the deposition process and relieving film stress.

The Si/SiC multilayer system has the best spectral selectivity of all the discussed multilayer structures: e.g., if we assume that line He II ($\lambda = 30.4$ nm) is six times brighter than proximate line Fe XVI ($\lambda = 33.5$ nm), a double-mirror telescope with Si/SiC coatings tuned to Fe XVI should yield a spectral contamination of only 2.7%, while the contamination corresponding to a Si/Mo MIS coating is 22%.

A new Be/Mg material pair has recently been proposed for use in the spectral region around 30 nm. The Be/Mg structure features a narrow spectral reflection band ($\lambda/\Delta\lambda \approx 20$). The use of an Al film with a thickness of 13 nm as a protective layer deposited onto the top Be layer provided an opportunity to achieve a record-high reflection coefficient (56%) and stabilize the structure [54].

Range: 35–50 nm

The region of EUV wavelengths longer than 40 nm covers several important lines of the solar spectrum (e.g., Ne VII with $\lambda = 46.5$ nm and O V with $\lambda = 63.9$ nm). Sc/Si [46,55] and SiC/Mg [45] multilayers have been proposed for visualization under normal incidence in the 25–50 nm wavelength range.

An ideal combination of excitations of valence and core electrons makes Sc the most promising element for MISs designed for wavelengths lying within the 35–50 nm interval. The Sc–Si pair was identified as the best coating [57–59] in the analysis of absorption spectra and calculated optical constants [56].

The reflection coefficient for Sc/Si mirrors under normal incidence is 30–54% [60]. However, the obtained values are not the limiting ones for Sc/Si coatings. Theoretical estimates and the results of electronic microscopic examination of Sc/Si interfaces reveal ample opportunities for further enhancement of their reflectance [55,60].

Mg/SiC multilayers operate efficiently in the wavelength range from 25 to 80 nm (and above). The absorption of Mg remains stable and low at these wavelengths. Combined with sharp and stable layer interfaces, this yields a peak reflectance of 30–50% under almost normal incidence angles. Mg/SiC features a unique combination of beneficial characteristics: high reflection coefficient, near-zero film stress, fine spectral selectivity, and thermal stability up to approximately 350°C. However, the Mg/SiC multilayer structure is prone to corrosion, which reduces the reflectance and makes it harder to utilize this structure in space solar telescopes.

The authors of [48,61] have demonstrated efficient corrosion-protection structures for Mg/SiC multilayers. They consist of nanoscale Al and Mg layers, which intermix spontaneously to produce a partially amorphous Al–Mg layer that makes a Mg/SiC MIS weather-resistant while preserving its unique combination of beneficial reflection characteristics.

The authors of [39] have also managed to prevent the intermixing of layers in a Si/Mg MIS by introducing barrier B_4C and Cr layers. The measured peak reflection coefficient and spectral selectivity for narrow-band mirrors based on Si/Cr/Mg/B_4C were $R \approx 30\%$ and $\lambda/\Delta\lambda \approx 30$, respectively [62].

Range: 50–121.6 nm

Spectral lines in the well-examined and densely populated 17–35 nm range may be contaminated by lines corresponding to higher or lower temperatures. Therefore, it seems rational to develop narrow-band multilayers for other EUV wavelengths where the lines of intermediate temperatures are isolated reliably. Isolated spectral lines covering a wide temperature range were discovered at longer EUV waves. For example, narrow-band imaging of the O V line ($\lambda = 62.97$ nm, 2.4×10^5 K) may fill the gap between the low-temperature He II line (8×10^4 K, $\lambda = 30.4$ nm)

and high-temperature lines, such as Fe XV (2×10^6 K, $\lambda = 28.4$ nm) and Fe XVI (3×10^6 K, $\lambda = 33.5$ nm) [63].

Lanthanides and similar elements have attracted the interest of researchers owing to a relatively low absorption in the long-wave EUV band [64]. These studies helped reveal those lanthanides that fit better the requirement of low absorption in the 50–115 nm interval. Multilayer systems based on Tb [65,66], Gd [63,67], and Nd [67] in combination with Si and SiC were developed as a result. At wavelengths exceeding 69 nm, multilayers based on La and B_4C with a diffraction peak at 90 nm have been reported [68]. La/B_4C MISs for the 70–115 nm range have been obtained; the development of more efficient multilayer films may also be expected.

A reflectance in excess of 20% under almost normal incidence has been observed for Si/Tb (SiC/Tb) MISs at a wavelength of 60 nm [65]. The maximum reflection coefficient of Si/Gd MISs designed for a wavelength of 62 nm was 26.2% at an incidence angle of 5° [63]. Two types of base materials are suited for operation in the $\lambda = 58.4$ nm spectral range (He I line). The first group is formed by materials with a high light reflection coefficient, a low absorption coefficient, and a small number of layers in the multilayer structure (e.g., rhodium (Rh) or ruthenium (Ru)). However, such mirrors have a very wide spectral transmission band. The other option is the use of relatively weakly absorbing metals, such as Mg or Al. It was demonstrated in [61] that Mg/SiC is a suitable material pair, since (i) the absorption of Mg remains relatively low in a wide range of EUV wavelengths from 25 nm (L absorption edge of Mg) to approximately 115 nm; (ii) Mg and SiC provide a fine optical contrast; (iii) Mg–SiC interfaces are sharp and stable. In the $\lambda = 58$ nm spectral range, the authors of [49] have analyzed a Mo/Mg multilayer structure; developed a number of MISs based on Mg/Al with barrier layers, such as Mg/Al/C and Mg/Si/Al/C (materials are listed starting from the substrate); and measured their reflectance.

The reflective characteristics of three-component Si/Al/Sc multilayer mirrors with a $MoSi_2$ cap layer as candidate systems for observation of the solar corona in the He I spectral line ($\lambda = 58.4$ nm) have been examined in [69]. A peak reflectance of 32% and spectrum width $\Delta\lambda = 5.4$ nm was achieved at 584 nm.

The Lyman-alpha line of hydrogen ($\lambda = 121.6$ nm) is the most intense EUV line of the solar spectrum; it is sensitive to variations of atmospheric structures forming at temperatures typical of the lower chromosphere/upper transition region (about 30000 K) [70]. An Al/MgF_2/B_4C multilayer coating and an Al/MgF_2 coating, which provides a reflection coefficient in excess of 75%, were used for the Lyman-alpha line in [71] and [70,72], respectively.

2.3. MIS optimization

Reduction of interface roughness

It follows from the above that the introduction of an antidiffusion barrier layer may contribute to smoothing of interfaces in certain cases. For example, a thin Mo layer introduced at the SiC-on-Al interface reduced its roughness and thus enhanced the optical properties of this system; Al/Mo/SiC multilayer interfaces became sharper than the Al/SiC system interfaces [36,38,73].

A common technique for fabrication of very smooth interfaces with minimum diffuse radiation scattering is ion polishing of each layer with the use of an individual ion gun following the process of ionic layer deposition [74] (or in the course of deposition) with ion energies of approximately two hundred electronvolts. This helps deposited atoms reach local positions corresponding to the minimum energy of the system [75,76]. Louis et al. [77] have reported on the successful application of ion-beam smoothing to coatings designed for the EUV range.

At first, Ar^+ ions were used in the majority of experiments on smoothing. However, owing to their small size, Ar^+ ions penetrate deep into layers and, consequently, may damage the interface below a layer. The use of larger ions, such as Kr^+ [78], appears to be a promising method for suppression of this effect.

The substrates onto which MISs are deposited exert a considerable influence on the reflection characteristics and imaging properties of MISs. In addition to the general requirement of atomic smoothness, substrates should satisfy certain requirements related to the specifics of tasks performed by a given MIS. The specifications of substrates, methods for their fabrication, and metrology techniques have been reviewed in [79]. The key materials for substrates with an ultralow expansion coefficient and silicon and silicon carbide substrates have been presented. Selected emerging substrate materials and fabrication technologies have also been discussed.

It was found that a negative bias potential (up to −200 V) applied to a substrate in the process of deposition of the silicon layer of a Mo/Si MIS makes the interfaces smoother and enhances the layer morphology [80].

A dependence of the interface roughness on the substrate temperature was observed in several experimental studies [81,82] into the optimization of Mo/Si MIS parameters.The minimum roughness corresponded to temperatures within the 120–250°C range. Cryogenic deposition of Mo/Si MISs has been performed by different research groups [83,84]. it was found that the roughness of mirrors deposited onto substrates kept at −155°C is lower than the roughness corresponding to room-temperature deposition. This is attributable to the fact that the nucleation rate at the initial stage of film growth is higher at lower substrate temperatures. The number of nucleation centers increases accordingly, and this translates into smoother interfaces.

Stress relief

The strict requirements imposed on MIS optics in the EUV range make it advisable to minimize the strain induced by the multilayer film stress. This strain may result in substrate bending or film delamination. However, the stress should be reduced or compensated without sacrificing the MIS reflectance. It was demonstrated that the film stress

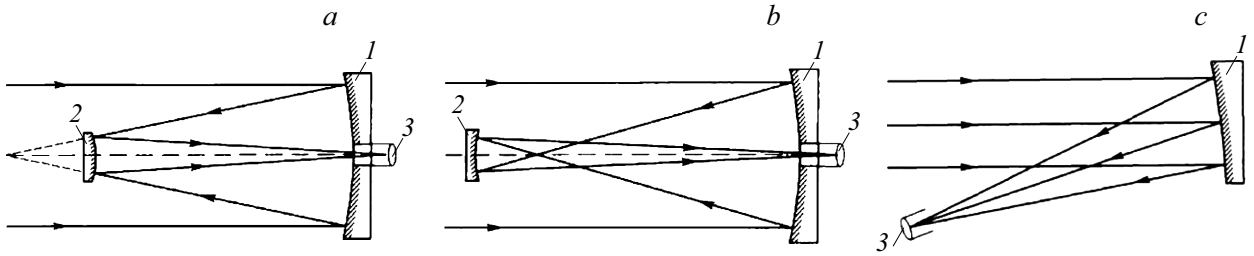

Figure 3. Optical circuits of Cassegrainian (a), Gregorian (b), and Herschelian (c) telescopes: *1* — primary mirror, *2* — secondary mirror, *3* — detector (see text).

may be controlled by adjusting the deposition conditions, such as nitrogenation [85,86] and argon pressure [87–89].

Other methods of stress reduction in Mo/Si multilayer films include post-deposition annealing [88,90–92], the introduction of stress-relieving buffer layers [88,93–95], and the adjustment of fraction γ [88,96–98].

It was found [98] that the stress values in Mo/Si MISs increase almost linearly with γ. It is known that the reflectance of Mo/Si MISs depends largely on parameter $\gamma = d_{\mathrm{Mo}}/d$ and reaches its maximum in the 13−13.7 nm spectral range at $\gamma \approx 0.42-0.44$ [98]. Varying the thickness ratio of Mo and Si, one may reduce the stress to near-zero levels at $\gamma \approx 0.6$; however, the reflectance also decreases considerably in this case ($R \approx 54-57\%$) [98].

2.4. Designs of normal incidence telescopes

The development of MISs opened up new opportunities for astrophysical solar research, since their narrow transmission bands coupled with high reflection coefficients allow one to perform diagnostics of the complete solar disk by imaging spectroscopy. The method is based on monochromatic imaging of the Sun in EUV lines with high angular, spatial, and temporal resolutions [99].

Multilayer normal incidence mirrors provide an opportunity to construct optical circuits of telescopes that are similar to the ones used in the visible spectral range. Figure 3 shows the optical circuits of Cassegrainian (a), Gregorian (b), and Herschelian (c) telescopes used in solar research.

In a Cassegrainian telescope, a larger concave (parabolic) primary mirror reflects rays toward a smaller convex (hyperbolic) secondary mirror (Fig. 3, a). The secondary mirror is installed between the primary mirror and its focus, and the total focal distance is greater than that of the primary mirror. The system is non-aplanatic (i.e., subject to coma aberrations).

It is well-known that aplanatic telescopes with zero (at least to the third order) coma and no spherical aberrations provide a higher efficiency in a much wider field of view. A Ritchey−Chrétien telescope, which is an aplanatic variant of the Cassegrainian configuration, utilizes hyperbolic primary and secondary mirrors [100].

In a Gregorian telescope, rays from a concave parabolic primary mirror are directed to a small concave elliptic mirror that focuses them onto a detector (Fig. 3, b). Since the elliptic mirror is located beyond the focal point of the primary mirror, the focal distance in a Gregorian telescope is larger than the one in a Cassegrainian telescope.

The primary mirror in a Herschelian telescope has the shape of an off-axis aspherical paraboloid and is tilted so that the focal point is outside the main telescope tube (Fig. 3, c). Compared to a double-mirror Ritchey−Chrétien telescope, which is considered to be the most promising for achieving a diffraction-limited angular resolution, a single-reflection Herschelian telescope is more efficient and simple and less sensitive to adjustment, but is larger in size [101].

Cassegrainian (MSSTA [102–104], TRACE [105,106], HiLiTE [107], XDT [108], AIA [27,46,109], and SUVI [110] telescopes) and Ritchey−Chrétien systems (EIT [111], MSSTA [100,102–104], EUVI [112], SPIRIT [113,114], SWAP [115,116]; ARKA [117,118], TESIS [39,62,119], and Hi−C [120] telescopes) are the ones used most often in astrophysics. Herschelian (MSSTA [102–104], SPIRIT [113,114], Solar Orbiter EUI [121,122]) and Gregorian (Solar Orbiter EUI [121,122]) systems are used less frequently.

Let us review briefly the specific features of certain telescopes. The MSSTA I observatory featuring seven Ritchey−Chrétien telescopes with an aperture of 127 mm, which operated in the wavelength range covering spectral lines H I, He II, C V, 0 VI, Fe IX/X, Fe XII, and Fe XVI; a Herschelian telescope with an aperture of 75 mm for the detection of Fe XII radiation; two Cassegrainian telescopes with an aperture of 62.5 mm, which reflected Fe IX/X and Fe XIV radiation; and four Herschelian telescopes with an aperture of 38 mm, which imaged bands dominated by emission lines Ne V, Si XII, and Fe XX, has been put into orbit in May 1991. The best MSSTA images have a resolution of $0.7''$.

The flight configuration of the MSSTA II observatory (launched on November 3, 1994) included six 127-mm Ritchey−Chrétien telescopes, one 127-mm and two 100-mm Herschelian telescopes, two 63-mm Cassegrainian telescopes, and eight 38-mm Herschelian telescopes. These modifications allowed MSSTA II to detect 17 images simultaneously in 17 transmission bands [103].

The concept of imaging at several wavelengths with a single multilayer coating may help reduce considerably

the cost, risk, and complexity of solar missions [123]. For example, the existing practice of imaging at several wavelengths consists in dividing each telescope mirror into several sectors that are tuned to different individual wavelengths. This approach requires developing several multilayer coatings and positioning a physical mask on top of a mirror in the process of multilayer deposition. In addition, several telescopes with a number of different EUV channels are needed in certain cases to achieve the scientific objective of a mission [48].

For example, the AIA instrument aboard the Solar Dynamics Observatory features four Cassegrainian telescopes and is designed for solar corona studies. Images are obtained almost simultaneously and cover at least 1.3 diameters of the Sun at several wavelengths with an angular resolution of $\sim 1''$, a field of view wider than $41'$, and a rate of 10 s (or higher). Each telescope produces images at two different wavelengths, since two different multilayer coatings are deposited onto two corresponding D-shaped regions of each mirror. Thus, a total of eight channels are provided: seven EUV ones (Table 1) and one ultraviolet channel. In each exposure, one half of the aperture is selected by blocking the other half with an aperture shutter or with the use of a filter positioned in the focal plane [27,46,109].

The mirrors of EIT [111], EUVI [112], and SPIRIT [113,114] Ritchey–Chrétien telescopes are divided into four sectors for successive imaging of the solar disk in four narrow spectral bands. Radiation passes through selector aperture *5* and selected filter sector *4* (Fig. 4). Filters suppress the greater part of ultraviolet, visible, and infrared radiation and block solar heat from entering the telescope. Radiation then enters one of the four optics quadrants. Each quadrant of the primary and secondary mirrors is coated with a narrow-band MIS optimized for one of the four solar spectrum lines.

Figure 5, *a* presents the solar disk imaged in the 304 Å channel (He II). This image has a granulation structure typical of the transition layer of the solar atmosphere with a temperature of $\sim 50\,000$ K. It was found in observations that the dynamics of this structure differs from the dynamics

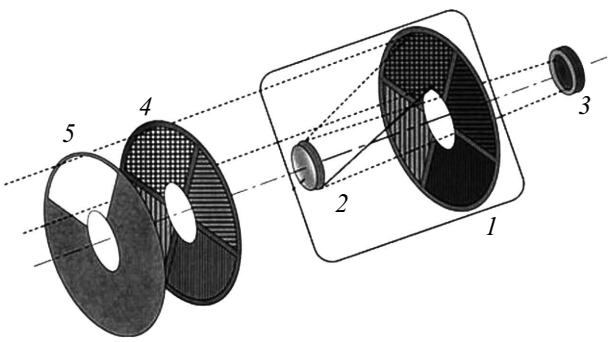

Figure 4. Diagram of the SPIRIT Ritchey–Chrétien telescope: *1* and *2* — primary and secondary mirrors of the Ritchey–Chrétien telescope, respectively; *3* — detector; *4* — input filters; *5* — selector aperture [114].

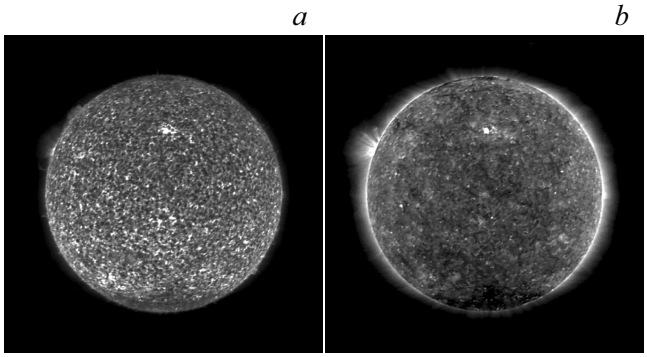

Figure 5. Images produced by the TESIS instrument in the 304 Å (spectral line of He II ions) (*a*) and 171 Å (spectral line of Fe IX ions) (*b*) channels [119].

of lower and cooler (chromosphere) and higher and hotter (corona) layers of the Sun. This suggests that different mechanisms and processes are at play in the transition layer. Observations in the 171 Å channel (Fig. 5, *b*) revealed various phenomena and processes occurring in the hotter (with a temperature around 10^6 K) and more dynamic corona region. The structure of this region differs radically from the structure of the transition layer, since the degree of plasma confinement is higher. The most distinctive coronal structures are seen clearly in Fig. 5, *b*: bright active regions and X-ray spots, above-limb arcades over active regions, and coronal holes (regions of reduced emission) [119].

The SUVI Cassegrainian telescope is the first EUV solar telescope with six channels having different multilayer coatings deposited onto each mirror [110]. All six coatings were deposited onto each mirror in the form of 60-degree segments that are tuned accurately to a specific EUV wavelength (Table 2) for „probing“ a certain temperature region of the observed solar atmosphere.

A double-band mirror coating for simultaneous detection of two emission lines has been proposed and optimized [123]. The coating in the FSI Herschelian telescope consists of a superposition of two periodic $[SiC/Mo/Al]^4/Al/[SiC/Mo/Al]^{30}$ MISs separated by a buffer layer. The first coating structure is an Al/Mo/SiC MIS, which utilizes first-order reflection ($\lambda = 17.4$ nm, 30 periods with $d = 8.95$ nm). An aluminum buffer layer and the second Al/Mo/SiC MIS are deposited on top of the first one. This second MIS utilizes first-order reflection ($\lambda = 30.4$ nm, four periods with $d = 16.5$ nm). The buffer layer thickness is optimized so as to achieve the desired shape of two Bragg peaks and suppress unwanted wavelengths [122].

3. Focusing hard X-ray radiation optics. Grazing incidence telescopes

Under normal incidence, the above-described approach, which is used widely in EUV solar research, may be extended to shorter SXR wavelengths that are suitable

Table 1. EUV wavelengths with the corresponding spectral lines and temperatures (T) used in the AIA instrument [46]

Channel, λ	MIS	$\Delta\lambda$	Spectral line	Solar region	Log (T)
335.4 Å	SiC/Mg	14 Å	Fe XVI	Active region corona	6.4
303.8 Å	SiC/Mg	13 Å	He II	Chromosphere, transition region	4.7
211.3 Å	Mo/Si	11.0 Å	Fe XIV	Active region corona	6.3
193.5 Å	Mo/Si	9.7 Å	Fe XII, XXIV	Corona and hot flare plasma	6.1, 7.3
171.1 Å	Mo/Si	7.4 Å	Fe IX	Quiet corona, upper transition region	5.8
131.0 Å	Mo/Si	4.8 Å	Fe XX, XXIII	Flaring regions	7.0, 7.2
93.9 Å	Mo/Y	1.1 Å	Fe XVIII	Flaring regions	6.8

Table 2. Calculated parameters of multilayer coatings for SUVI [110]

Wavelength (Å)	93.9	131.2	171.1	195.1	284.2	303.8
Coating materials	Mo/Y	Mo/Si	Mo/Si	Mo/Si	Mo/Si	Mo/Si
Bilayer thickness d (Å)	47.80	67.15	88.35	102.00	152.50	165.00
Number of bilayers	120	50	40	40	20	20
$\gamma = d_{Mo}/d$	0.35	0.36	0.175	0.15	0.15	0.15

for observations of both galactic and extragalactic X-ray radiation sources [99,124]. Telescopes with grazing incidence optics are commonly used to study astronomical objects radiating in the SXR range [1]. A considerable progress in visualization is associated with the construction of telescopes capable of focusing radiation with an energy of 10–200 keV (i.e., in the range where normal incidence X-ray telescopes are unsuitable for use due to the infeasibility of fabrication of MISs with a small bilayer size, while the applicability of grazing incidence telescopes is limited by the smallness of the critical angle of total external reflection of HXR and gamma radiation). However, a fine reflectance at above-critical grazing angles may be achieved through the use of MISs. Thus, multilayer and grazing incidence optics may complement each other and be combined efficiently in a hybrid system for various astronomical applications.

However, in contrast to narrow-band EUV optics used in solar astrophysics, efficient HXR- and gamma-focusing optics needs to be wide-band.

3.1. Depth-gradient MIS

A more efficient option for enhancing the MIS transmittance consists in adjusting the d-interval in such a way that radiation with different energies is reflected at different depths within an MIS. Thus, the fabrication of a multilayer structure with its period varying smoothly with depth is an obvious opportunity for expanding the transmission band [125–130]. Shorter-wavelength radiation is then diffracted at deeper layers of the structure, since it normally has a lower absorption coefficient (Fig. 6).

A well-known method of construction of an aperiodic MIS consists in reducing the d-interval gradually in accordance with a power law [125]:

$$d(j) = a/(j+b)^c, \tag{6}$$

where $j = 1, 2 \ldots n$ is the index of bilayer j. Coefficients a, b, c, number of bilayers N, and thickness fraction γ need to be optimized in order to achieve the desired reflectance dependent upon the photon energy. Parameter γ of gradient MISs, which are often called supermirrors, may be a constant or a slowly varying quantity that is set for the purpose of optimizing the reflection efficiency (i.e., finding

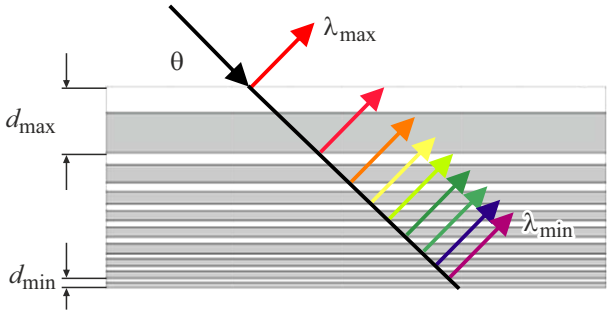

Figure 6. Schematic diagram of a depth-gradient MIS [130].

the best compromise between constructive interference and photoelectric absorption [131]).

The block method, which consists in the application of blocks with constant d [132], is another possible technique for constructing gradient MISs. In order to reduce the absorption of such structures, the block reflecting radiation with the lowest energy should be positioned on the surface. Blocks located deeper within the structure facilitate the reflection of X-rays with higher energies.

Multilayer coatings for X-ray and gamma telescopes have the potential to enhance their reflectance considerably. This approach, which has already been discussed and examined in [4,125,132,133], is of special interest, since it allows one to carry over the characteristics and achievements of technologies developed for SXR focusing optics to HXR and soft gamma optics.

The requirements imposed on optical constants of elements of gradient MISs depend on the applied optimization criterion and, generally speaking, differ from those corresponding to periodic mirrors. However, material pairs yielding the best results in periodic MISs often also perform well in aperiodic structures.

Materials chosen for multilayer structures with a depth-graded period for X-ray telescopes ($10\,\text{keV} < R < 100\,\text{keV}$) were targeted at W/Si, W/SiC, Pt/C, and Pt/SiC MISs [134]. These material combinations were chosen for their fine temporal stability and low interface roughness. However, the absorption edges of both W and Pt fall within the 70–80 keV range. Judging by their optical constants, Cu and Ni should be fine candidates for replacing materials with high values of atomic number Z, since the K absorption edges of Cu and Ni are below 10 keV. Among the alternatives to W/Si are Cu/Si [135], Mo/Si, Ni/C, Pt/C, as well as NiV/C and NiV/SiC structures [136]. All of them (except for the Pt/C MIS, the applicability of which is limited by the K absorption edge of Pt (78.4 keV)) are capable of wide-band reflection of photons with energies from 20 to 100 keV. Although Pt/C and Ni/C provide excellent efficiency figures, silicon has a higher deposition rate than carbon; this makes the Cu/Si system appear to be the better choice for mirrors reflecting radiation with energies above the K absorption edge of W (69.5 keV) [126].

Since WC/SiC coatings allow for very small d-spacing values [137], a combination of WC/SiC (or well-proven W/SiC) with the above-mentioned Cu- and Ni-containing multilayers in a single two-component MIS block allows one to develop new designs for X-ray and soft gamma telescopes [138].

3.2. Telescopes based on gradient MISs

The first astronomical observations with HXR radiation have been performed in the InFOCμS balloon-borne experiment in 2001 and 2004 [139–141]. X-ray images in the energy range from 25 to 45 keV have been obtained with the use of gradient Pt/C multilayers deposited onto mirrors in the Wolter I geometry. This geometry is used widely in SXR telescopes and combines two types of grazing incidence mirrors (primary paraboloidal and secondary hyperboloidal mirrors) with their surfaces being revolving ones [142]. The suppression of optical aberrations, such as coma, is an advantage of a system of double mirrors. In order to enhance the effective collection area of an X-ray telescope, several interleaved mirror shells are combined (Fig. 7) [143]. The costly Wolter I optical arrangement with hard-to-fabricate mirrors may be substituted with a conical Wolter I configuration where the parabola and the hyperbola are approximated by a double cone [144]. This solution helps reduce considerably the cost and complexity of fabrication of mirrors, but the angular resolution is sacrificed.

In most cases, the optics of telescopes designed for HXR celestial observations is a conical approximation of the Wolter I geometry. Different methods of fabrication of optical systems, substrate materials [1], and compositions of gradient MISs may be used. For example, the focusing optics of HEFT [145–151] and NuSTAR [151–159] telescopes is based on multilayer gradient coatings deposited onto thermally shaped thin glass mirror segments [160–162].

HEFT has been launched on May 18, 2005, into the upper atmospheric layers on a balloon. The telescope consists of several individual modules. Each module contains 72 closely interleaved mirror shells with a thickness of 0.3 mm and a radius from 40 to 120 mm. Each mirror shell is divided into five mirror segments (Fig. 8). Thus, a telescope module consists of 1440 mirror segments [150]. Each segment is coated with a gradient MIS deposited by planar magnetron sputtering. W/Si and Ni/C multilayer structures are used at outer and inner shells, respectively.

NuSTAR has been put into orbit on June 13, 2012, with two co-aligned and independent telescopes. Each of them features an optical module and a CdZnTe detector (separated by a 10-meter extendable mast) in the focal plane. The NuSTAR mission is an extension and upgrade of the balloon-borne HEFT design, which was experimentally proven to be efficient, and is the first focusing high-energy X-ray telescope in orbit. NuSTAR operates in the 3–79 keV photon energy interval, thus expanding the range of

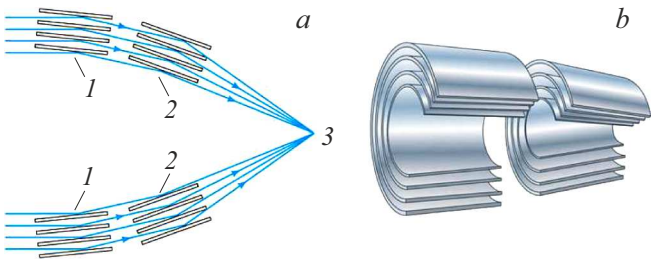

Figure 7. Propagation of X-rays in a multilayer Wolter I mirror: rays are reflected successively off parabolic *1* and hyperbolic *2* surfaces of each mirror shell to establish focal point *3* (*a*). Three-dimensional schematic representation of mirror shells in the Wolter I configuration (*b*).

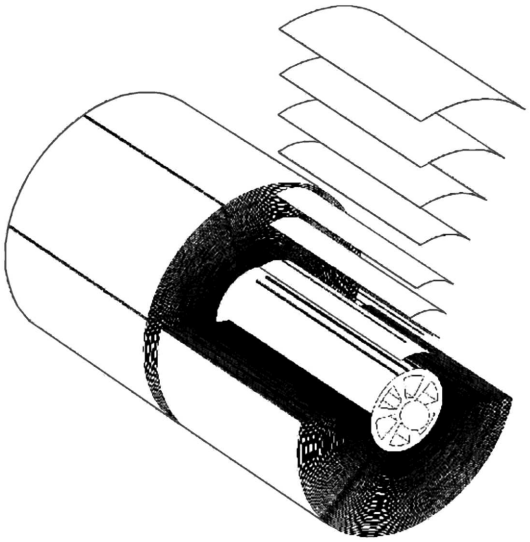

Figure 8. Assembly geometry of a HEFT telescope module. A total of 72 shells are constructed from individual glass segments with the use of precision machined graphite spacers [147].

telescopes well beyond the limit of 10 keV that was typical of all the earlier X-ray satellites.

Each NuSTAR optical module contains 133 interleaved mirror shells. Each shell consists of 12 or 24 thin (0.2 mm) glass segments (depending on the optics radius). The inner 89 shells are coated with a gradient Pt/C multilayer structure, which remains efficient at photon energies below the K absorption edge of Pt. The outer 44 shells are coated with a W/Si multilayer structure, which remains efficient below the K absorption edge of W. The angular resolution of NuSTAR is as high as $40''$, while the resolution of HEFT optics did not exceed $1.5'$ [151].

The optics of InFOCμS [139–141,163] and ASTRO-H [164–166] telescopes is based on thin aluminum segments coated with Pt/C MISs.

InFOCμS is a balloon-borne telescope project for observation of a cosmic hard X-ray source. The telescope optics is designed for operation in the 20−80 keV range (the lower energy limit, 20 keV, is set by atmospheric absorption, while the upper limit corresponds to the K absorption edge of platinum) and features 255 interleaved thin (0.17 mm in thickness) mirror shells.

The ASTRO-H Japanese astronomical X-ray satellite has been put into orbit on February 17, 2016. It is fitted with two identical hard X-ray telescopes (HXT) that cover an energy range of 5–80 keV. The focal distance of HXT optics is 12 m. A total of 213 cylindrical mirror shells with a thickness of 0.2 mm, a diameter of 120–450 mm, and a length of 200 mm are used to produce a greater effective area.

HEX-P [167,168] — is a next-generation telescope concept that expands considerably the capabilities of wide-band X-ray observatories. Working in the 2−200 keV energy range, HEX-P should provide a 40 times higher sensitivity than any earlier mission in the 10−80 keV range and should become the first focusing instrument to operate in the 80−200 keV range. The extension of sensitivity to $E \sim 200$ keV is of particular interest, since several key nuclear transitions of radioactive elements produced in supernova explosions lie between 50 and 200 keV. For example, decays of ^{44}Ti (68 and 78 keV) and ^{56}Ni (158 keV) are of interest, since the production and ejection of ^{44}Ti are sensitive to the explosion mechanism, and the temporal evolution of intensity of the ^{56}Ni line is sensitive to the structure and dynamics of ejection [147].

The projected angular resolution of the HEX-P telescope in terms of half-power diameter (HPD) is $15''$, which is regarded as a goal attainable within the next decade [169] (HEX-P is to be launched in 2031).

HEX-P will be comprised of three modules focused on separate detectors. The state-of-the-art technology of fabrication and assembly of HEX-P mirrors involves polishing of single-crystal silicon plates and their modular assembly [169]. A total of ~ 50000 small mirror segments $100 \times 100 \times 0.25$ mm in size will be fabricated, coated with gradient MISs (hybrid W/C + Ni/C coating is expected to be used to expand the transmission band from 80 to 200 keV), and integrated into 42 modules, which will then be assembled into nine meta-shells. These, in turn, will be integrated into three identical mirror assemblies.

4. Focusing optics for soft gamma radiation. Laue lens

Celestial observations in the gamma range provide an opportunity to identify the most intense sources and the most turbulent events in the Universe. While lower-energy wavelength ranges are normally dominated by thermal processes, gamma radiation allows one to image the nonthermal Universe. Here, nuclear reactions synthesize the key components of our world, and particles are accelerated to ultrarelativistic energies via mechanisms that still remain understudied. Cosmic accelerators and cosmic explosions are the primary research topics related to gamma observations.

Recent technological advances in focusing of gamma rays with the use of diffraction techniques have paved the way for scientific missions that offer considerably higher sensitivity and angular resolution parameters than the earlier ones [170]. These future gamma-imaging projects should provide an opportunity to examine the processes of particle acceleration and explosion physics in unprecedented detail, thus offering valuable insights into the nature of the most turbulent and energetic processes in the Universe [171].

4.1. Structural features of a Laue lens

The best technique for focusing of soft gamma radiation is diffraction in the transmission (i.e., Laue) geometry. Specifically, a Laue lens focuses gamma rays using a large

Table 3. Parameters of eight rings with Ge crystals (lattice parameter $a = 5.65$ Å) of the Laue lens for focusing of photons with an energy of 170 keV ($f = 277$ cm) developed for CLAIRE [177]

Ring	Plane (hkl)	$d(hkl)$, Å	Number of crystals	Radius, mm	Bragg angle
1	111	3.27	28	61.7	0.64°
2	220	2.00	52	100.8	1.04°
3	311	1.71	56	118.2	1.22°
4	400	1.41	72	142.6	1.48°
5	331	1.30	80	156.2	1.61°
6	422	1.15	88	174.7	1.81°
7	333	1.09	96	188.2	1.92°
8	440	1.00	104	201.7	2.09°

number of crystals that are positioned and precisely oriented in concentric rings [5,172–175] (Fig. 9). This principle is applicable at photon energies from 100 keV to 1.5 MeV.

If photons reflected off all crystals are to be focused properly into a single point, the direction of the diffraction vector of each crystal should cross the lens axis, and this vector should be tilted by Bragg angle θ relative to the focal plane. Angle θ also defines the energy of reflected photons and depends on distance r between the crystal center and the lens axis (and on focal distance f). The outer lens radius and the focal distance specify the minimum energy that may be focused by a given crystalline material [176].

One may distinguish two subclasses of crystal diffraction lenses: Laue lenses with a narrow transmission band and wide-band Laue lenses. In narrow-band Laue lenses (e.g., CLAIRE), each crystal ring utilizes its own set of lattice planes $[hkl]$ for focusing of photons of one energy band into a common focal spot. Radius r_i of ring i of a lens with a given focal distance f is written as

$$r_i = f\tan[2\theta_i] \approx f\lambda d_i, \qquad (7)$$

where d_i is the interplanar distance of crystals of ring i and λ is the radiation wavelength.

Table 3 lists the parameters of the narrow-band Laue lens developed for the balloon-borne CLAIRE telescope [177]. This lens is made up of germanium crystals positioned in eight concentric rings.

A single set of lattice planes with the optimum diffraction efficiency may be used in a wide-band diffractive lens. Owing to a difference in Bragg angles, each concentric ring of crystals focuses photons with an energy that differs somewhat from the energy of photons focused by crystals of the neighboring ring. Thus, a lens of this type may cover a wide energy band. If crystals of ring *1* are tuned to the diffraction of photons with energy E_1, diffraction planes of ring *2* should be tilted slightly more relative to the incident ray in order to reflect energy $E_2 < E_1$ to the same focal point (Fig. 9).

Apparently, the best configuration of crystals is achieved when they are arranged in an Archimedean spiral that

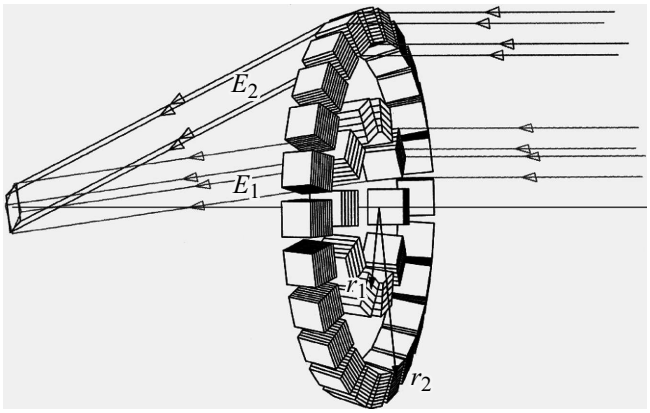

Figure 9. Path of rays with energies E_1 and E_2 ($E_1 > E_2$) in a Laue lens. The focal spot is a projection of crystals onto the focal plane [177].

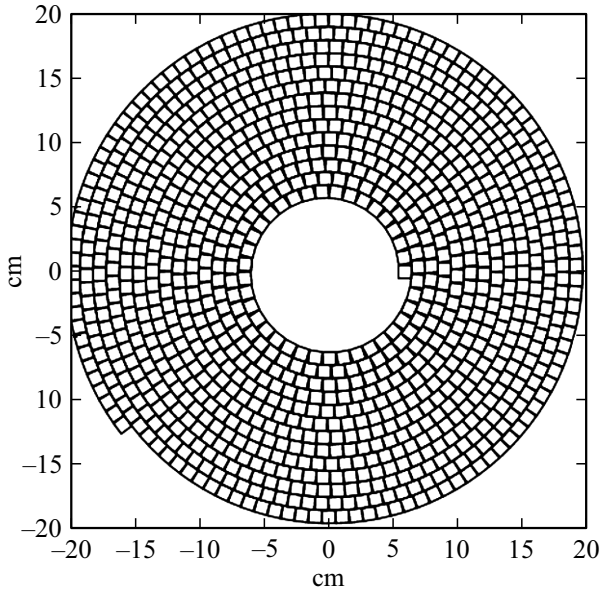

Figure 10. Configuration of a prototype Laue lens with crystals arranged in an Archimedean spiral. The lens size corresponds to a focal distance of 210 cm and a nominal transmission band of 60−200 keV [179] (see text).

provides a smoothly varying value of r (Fig. 10). It was demonstrated [178–180] that, if the interplanar distances of all crystals of a lens are the same, this arrangement yields a smooth variation of the effective data collection area with energy and eliminates jumps associated with the contributions of higher diffraction orders [179,180].

However, Laue lenses consisting of a set of rings are inherent to the concepts of GRI [181,182], CLAIRE [177], MAX [183,184], DUAL [185], and ASTENA [186] missions. Since rings of different radii focus radiation to a single point, the Bragg angle varies from one ring to another.

4.2. Crystals for a Laue lens

In order to provide continuous coverage of a wide energy range, crystals of each ring should feature a sufficiently wide transmission band that overlaps with the transmission bands of neighboring rings. Therefore, perfect crystals are normally substituted with mosaic ones or crystals with bent diffraction planes [181,187].

Mosaic crystals

A mosaic crystal is an agglomerate of crystalline blocks. Each block is perfect in itself, but neighboring blocks are slightly misaligned. The peak reflection coefficient of such a crystal is lower than the one of a perfect crystal; however, the integrated reflection coefficient of a mosaic crystal is higher, and it maintains a considerable reflectance in a range of angles that may exceed substantially the angular width of reflection of a perfect single crystal. The angular distribution of blocks may be approximated by a continuous function. It is assumed that this function is Gaussian with FWHM Ω, which is called the mosaic spread. A detailed description of diffraction in mosaic crystals was provided by Zahariasen [188].

The energy transmission band of a crystal and, consequently, the whole ring is written as

$$\Delta E_i = 2\Omega E_i f / r_i. \quad (8)$$

The minimum value of Ω for crystals as a function of the focal distance and radial ring size r_i of crystal plates is given by [181]

$$\Omega \geq (r_{i+1} - r_i)/2f. \quad (9)$$

The quality criteria for a mosaic crystal are the mosaic spread, which should fall within the range from $10''$ to $60''$, the diffraction efficiency, homogeneity, and reproducibility. The mosaic spread needs to be maximized to achieve the highest possible transmittance of a lens. However, it should be kept in mind that the spatial resolution and the sensitivity of a telescope are limited by the so-called mosaic defocusing effect [172,174,189].

In a first approximation, the diffraction efficiency of a crystal increases with its electron density. However, a more rigorous analysis requires examining the geometry of the crystal lattice and radiation absorption, which increases with Z and decreases at higher photon energies [173,187,190].

Crystals of copper, gold, germanium, and silicon–germanium alloys have already been used as diffraction elements for Laue lenses. For example, $Si_{1-x}Ge_x$ crystals with a composition gradient and Cu and Au mosaics performed remarkably well: their reflectance was as high as 31% at 600 keV (Au) or 60% at 300 keV (SiGe), and the angular spread was as low as $15''$ (Cu). These parameters satisfy well the requirements for application in Laue lenses [187]. The characteristics of $Ge_{1-x}Si_x$ ($x \approx 0.02$) crystals grown in accordance with the modified Czochralski technique were reported in [177]. The mosaicity of these crystals fell within the range from approximately $30''$ to $2'$.

The possibility of growth of crystals with a well-defined mosaicity or dislocation density is a crucial point. Dislocation-free high-quality germanium crystals are available at present; therefore, the needed degree of mosaicity may be set deliberately in the process of growth [191] or post-growth treatment [192,193]. Germanium crystals with a mosaic spread of 0.2–1.5° may be produced [191] via high-temperature plastic straining, but it is difficult to control the accuracy of this parameter (especially in the mosaicity range from $1'$ to several tens of angular seconds).

The authors of [194] have concluded that GaAs crystals with a certain mosaic spread may be grown under properly adjusted growth conditions (specifically, the thermal gradient at the solidus–liquidus interface, the stoichiometric deviation of the melt, or the dopant concentration).

In general, mosaic copper and germanium crystals are the ones used most often in the design and fabrication of Laue lenses. For example, the fabrication of a Laue lens consisting of 600 germanium single crystals (cubes with a side length of 0.93 cm), which utilize diffraction planes [111], [220], [311], [400], [331], [422], [333], and [440] are were mounted in eight concentric rings, has been reported in [195].

The Laue diffraction lens of the MAX mission will consist of 13740 copper and germanium crystals ($Ge_{1-x}Si_x$, $x \sim 0.02$) arranged in 36 concentric rings. It will focus photons in two energy bands simultaneously. Each of them will serve to fulfill one of the primary research objectives: the 800−900 keV band is expected to be used for examining nuclear lines of gamma radiation of type Ia supernovae (e.g., the ^{56}Co decay line at 847 keV), while the 450−530 keV band is proposed to be used for the study of electron–positron annihilation. Cu (111), Cu (200), Cu (220), Cu (222) (18 rings), and Ge (311) (2 rings) crystals are meant to cover the 800−900 keV band, while Cu (111), Cu (200) (14 rings), and Ge (111) (2 rings) should cover the 450−530 keV band [184].

Bent crystals

However, while crystals offer an advantage of fairly simple fabrication in large quantities with fine reproducibility in terms of size and mosaic spread, they have their limitations, which may be summarized as follows:

(1) even if the absorption of radiation by crystals is neglected, their efficiency is limited to 50% due to the equilibrium between direct and diffracted beams [188];

(2) the size of an image in the focal plane depends primarily on the size of a crystal and the degree of its mosaicity: a large mosaic spread may lead to defocusing.

Crystals with bent diffraction planes are an alternative to mosaic crystals and have the potential to overcome these two limitations. First, their energy range is proportional to the curvature radius and may thus be controlled accurately, and their diffraction efficiency is unlimited [187,196,197], since a continuous variation of the incidence angle at bent lattice planes prevents repeated diffraction [198].

Second, given the fact that crystals with bent lattice planes yield a focal point smaller than the cross section of a crystal itself, such crystals may overcome the focusing limitation of planar mosaic crystals.

Bent crystals also have an advantage in that their diffraction profile is rectangular with a width specified by the curvature radius, while mosaic crystals have a Gaussian diffraction profile with a FWHM equal to the mosaic spread. Since Gaussian tails are lacking, bent crystals are better at focusing soft gamma radiation [199]. Crystals of this type may be fabricated in a number of ways [190].

Controlled mechanical damaging of one surface of a crystal (e.g., by polishing [199,200] or grooving (Fig. 11) [198,201]) is one of the common methods for fabrication of bent crystals. This method relies on plastic straining of a crystal induced by grooving of one of its largest surfaces: the surface damage introduces defects into a surface layer with a thickness of several tens of micrometers that is subjected to compressive strain [202,203]. A uniform curvature is produced as a result of straining without the need for any external influence. This method is cheap, simple, and fit for mass production.

The mentioned methods are fit for mass production, but inevitably inflict considerable damage to crystals [201]. Ion implantation [204] and sandblasting [205] have also been proposed to be used for crystal straining. Both methods produce compressive stress at the crystal surface, thus inducing controlled matrix straining. However, they do not allow one to bend thick crystals, which are preferable for Laue lenses [206].

A method for fabrication of thick bent crystals by depositing carbon fiber layers onto the crystal surface has been proposed recently. Curvature is then produced due to the difference in thermal expansion coefficients of a crystal and a carbon fiber composite: the composite has the capacity to establish a stress field that bends the crystal after polymerization [206,207].

A bent crystal may also be formed using the concentration gradient method (i.e., by growing a two-component crystal with a gradient composition along the growth axis [208,209]). For example, bent crystals of a GeSi alloy with an initial germanium concentration of 3–7% were fabricated by altering the mixture composition during growth [210,211]. However, it is rather hard to grow crystals in this fashion. The method is hardly applicable to Laue lenses, since crystals need to be mass-produced in this case [212].

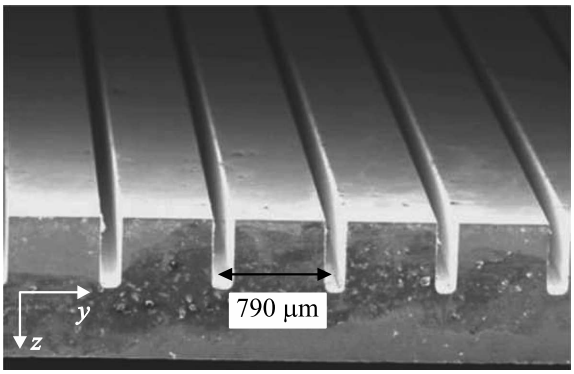

Figure 11. A section of a bent silicon crystal (side view) with a series of grooves imaged with a scanning electron microscope. The arrow denotes the groove pitch [201].

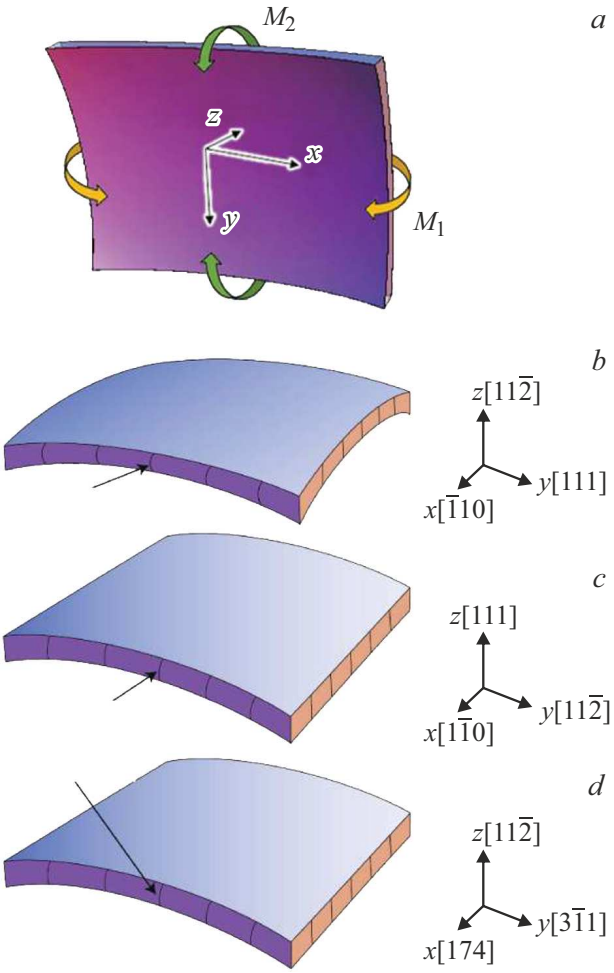

Figure 12. Schematic diagram of a crystal plate with the coordinate system used for modelling. *a*: Bent arrows denote applied moments M_1 and M_2. Two moments (*b*) or one moment (*c*, *d*) may be applied. Arrows point at bent lattice planes [215].

Quasi-mosaic crystals

Anisotropic strain, which induces the so-called quasi-mosaicity (QM) effect [213,214], may be used efficiently within the concept of bent crystals. The concept of QM is crystals has been examined from a number of angles (including the theoretical background and fabrication techniques) in [215].

The elasticity tensor of a crystalline material may contain off-diagonal elements. Thus, nontrivial strain may emerge under the influence of external forces. A crystal plate under

the influence of two mechanical moments M_1 and M_2, which are applied about axes y and x (Fig. 12, a), is subjected to primary strain. The emergence of secondary curvature depends on the crystal anisotropy. Thus, the primary and secondary curvature radii are strongly connected to the crystal orientation. Most importantly, quasi-mosaicity allows one to focus a photon flux into a point smaller in size than the diffracting crystal (i.e., with a high overall efficiency). This is difference between diffraction by a QM crystal and diffraction by traditional mosaic or bent crystals, which form a focal point that is no smaller in size than the crystal itself. Therefore, since the focal point may be adjusted in size by varying the secondary curvature, QM crystals provide an opportunity to focus photons with a high angular resolution, thus enhancing the sensitivity of Laue lenses. The primary curvature of a QM crystal accounts for focusing of a photon flux, while the secondary curvature enhances the overall diffraction efficiency [216]. The sensitivity of a Laue lens may be increased as a result [217,218].

The authors of [219] and [220] have observed experimentally the diffraction of X-rays by planes (111), which were bent due to the QM effect (Fig. 12, b), of Si and Ge crystals, respectively. Experimental evidence of diffraction of X-rays by a Si sample with reflecting planes $(11\bar{2})$ bent due to the QM effect (Fig. 12, c) and with planes $(3\bar{1}1)$ (Fig. 12, d) has been obtained by the authors of [217] and [218], respectively. QM crystals are already coming into use. For example, Si and Ge crystals with reflecting planes (111), a cross section of 30×10 mm, and a curvature radius of 40 m are expected to be used in the ASTENA mission telescope [186].

4.3. Design and assembly of a Laue lens

The selection and arrangement of crystals are crucial for fabrication of an efficient Laue lens. Since a lens may be very expensive, the issue of proper simulation of its operation prior to fabrication is a crucial one. However, the problem of optimum positioning of crystals in a Laue lens cannot be solved analytically [221]. A genetic algorithm may be the best method to solve this problem. This algorithm is a heuristic search that imitates the process of natural selection. Specifically, a Laue lens may be optimized using a pseudo-evolutionary process that favors the best crystals and thus directs the system to a configuration with the needed parameters. For example, the *LaueGen* algorithm is a method for selecting an arranging crystal planes in a Laue lens in a way that maximizes the integrated reflectance while smoothing the energy dependence of collected photons. The spectral response smoothing is crucial to simplifying the deconvolution of the signal received, while a high reflectance of optical elements is instrumental to enhancing the signal-to-noise ratio of a lens [221]. Regardless of the choice of crystals, the efficiency of focusing of a Laue lens in a given energy range is defined by the following three key parameters: focal distance, crystal size, and mosaicity of crystals [222]. The requirements as to the accuracy of alignment of crystals depend strongly on the focal distance and the mosaicity of crystals used. This is attributable to the fact that the sensitivity of a telescope with a Laue lens increases with increasing focal distance and decreasing crystal mosaicity [222,223]. However, a very accurate alignment of crystals is needed to achieve a large focal distance and reduce the mosaicity. If one fails to do so, the efficiency of a lens may decrease significantly. Therefore, the development of a technique for assembly of a large number of crystals into a lens with an adequate alignment accuracy is of key importance [174]. The methods for assembly and alignment of crystals have been reviewed in [176,224–228].

5. Focusing optics for X-ray and gamma radiation. Fresnel zone plates

Certain important scientific questions may be answered only through observations with X-ray telescopes with a very high angular resolution.

These issues include the examination of the medium surrounding supermassive black holes, pulsar wind nebulae, various stages of stellar evolution, etc. Diffractive optics (specifically, Fresnel zone plates (FZPs) [6,7]) technically allows one to construct large diffraction-limited and efficient X-ray and gamma telescopes that may provide a massive improvement in angular resolution.

An FZP consists of a series of concentric circular zones that alternately absorb and transmit radiation (Fig. 13, a). The focusing effect is achieved by means of interference of waves passing through non-absorbing zones. Since diffraction always produces several orders, they also need to be considered in the case of an FZP.

FZP efficiency η_m is the fraction of photons incident on an optical element and focused in diffraction order m:

$$\eta_m = 1/(\pi m)^2. \qquad (10)$$

In the first diffraction order, the maximum efficiency of π^{-2} ($\sim 10\%$) corresponds to a traditional („classical“) FZP. Only the first diffraction order ($m = 1$) is used in most cases, since it is the brightest one. Phase FZPs are used to enhance the efficiency.

In theory, the so-called kinoform FZP [229] with a parabolic zone profile performs ideal phase modulation: it does not only exert a constant phase shift in neighboring zones, but also carries out continuous transformation of an incident planar wave front into a spherical one that converges in focus. In addition, kinoform lenses offer the combined advantage of a low background signal and efficient suppression of unwanted higher diffraction orders. The theoretical maximum focusing efficiency of an FZP with a parabolic profile (Fig. 13, b) is 100% (if radiation absorption is neglected).

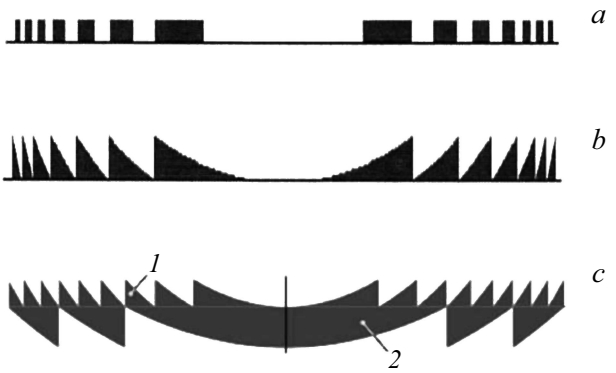

Figure 13. Profiles of different configurations of focusing diffractive instruments: „classical" FZP (*a*); phase FZP with a parabolic zone profile (*b*); monolithic achromatic doublet with a kinoform profile of the diffractive component (*1*) and a stepped profile of the refractive (*2*) component [238] (*c*).

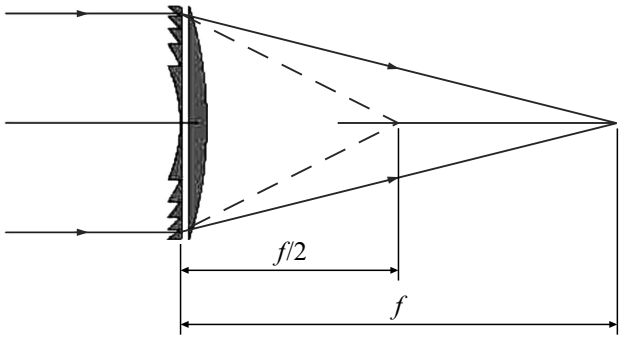

Figure 14. Using a refractive lens to compensate chromatic aberration of the first order in an FZP [232].

The effective angular resolution of a telescope with an FZP with diameter D and focal distance f operating at energy E is specified by a combination of three factors: diffraction-limited angular resolution $\theta_d = 1.22\lambda/D$; limiting spatial resolution $\theta_s = \Delta x/f$ of the detector (Δx is the spatial resolution of the detector); and limiting chromatic aberration $\theta_{\Delta E} = 0.2(\Delta E/E)(D/f)$ (ΔE is the width of the FZP energy band) [230].

An achromatic diffractive–refractive X-ray lens [230–238] has been proposed to reduce the contribution of chromatic aberration to the effective angular resolution in X-ray and gamma astronomy. It consists of a diffractive FZP with focal distance f_d in close contact with a diverging lens (i.e., convex refractive component) with focal distance f_r. When these two components are in direct contact, they act as a single instrument. The dependences of the focal distance of the FZP and the refractive lens on the radiation energy are linear and quadratic, respectively. Therefore, the focal distance of a contact pair as a function of energy remains unchanged at an energy for which focal distance f of the lens is two times larger than the focal distance of the FZP: $f_d = f/2$ and $f_r = -f$ (Fig. 14). This requirement may be satisfied at any photon energy if one chooses the proper lens parameters. Thus, there exists an energy band with a maximum at which chromatic aberration of the first order may be corrected [232,239]. In this context, the energy band width increases from $\Delta E = E/N$ (N is the number of zones) for a „classical" FZP to $\Delta E = E/N^{1/2}$ for an achromatic lens [236].

If a doublet is split, the emerging degree of freedom provides an opportunity to correct chromatic aberration of both the first and the second orders [232]. It is often preferable from absorption considerations to impart a stepped profile to the refractive component, thus effectively transforming a lens into a monolithic achromatic doublet [238] (Fig. 13, *c*).

It has been proposed to use phase FZPs in X-ray telescope designs optimized for observations of solar flares [240] and the study of phenomena occurring in the immediate vicinity of black holes and neutron stars [241]. Since an achromatic doublet has a limited energy transmission band, six diffractive–refractive lenses are expected to be used in the *MASSIM* mission to cover the needed 4.5−11 keV energy range, which was chosen so as to contain important Fe lines. Each lens will have a diameter of 1 m and an excellent angular resolution ($\sim 2 \times 10^{-3''}$) and will provide an effective collection area of several thousand cm^2 [241].

The equation for focal distance

$$f = 4N(\delta r_N)^2/m\lambda \qquad (11)$$

demonstrates that if a certain reduction in angular resolution is permissible, the focal distance may be shortened in operation at a lower energy E by reducing the size of the outer FZP zone (δr_N) or the zone number (N). For example, segmented designs of Laue lenses have been proposed [236,237,242] to reduce the number of zones and simplify the retargeting of a telescope. A lens is divided into optically independent circular segments. Each of these rings is divided into sections of equal size (Fig. 15). Note that a segmented FZP is similar in terms of design to a Laue lens.

The concept of efficient simultaneous visualization in five energy ranges from 5 to 10 keV in a high-resolution X-

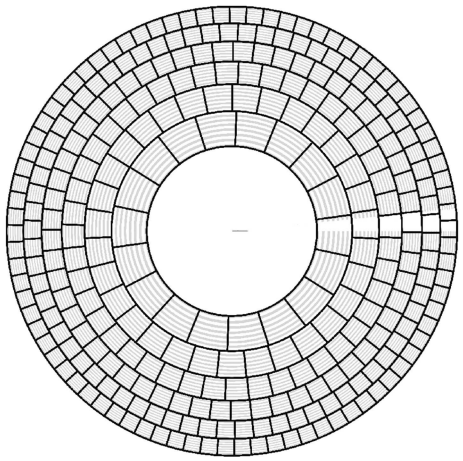

Figure 15. Possible design of a segmented FZP [239].

ray telescope has been detailed in [237]. This design is optimized for a shortened focal distance ($\sim 10^2$ km). The use of a segmented achromatic lens allows one to arrange efficiently several ring apertures for close energy bands. A typical focal spot size of ~ 1 mm translates into an angular resolution of approximately $10^{-3}''$ within the entire spectral range. The total spectral width covered by a multiband telescope is more than 1 keV (or 1/4 of the overall range from 5 to 10 keV). Therefore, it will be of particular interest to apply the proposed achromatic instrument to wide-band X-ray radiation sources. This telescope will have a detector mounted aboard a separate spacecraft and will allows for fast reorientation to new astrophysical targets.

The launch of a telescope with a large focal distance implies operating two spacecraft (one with focusing optics and one with a detector in its focal plane) with active control of their mutual positioning. Certain issues related to the flight operation of an X-ray diffraction telescope of this type have been discussed briefly in [230,243]. The results of studies reported in [244,245] confirmed that such an ambitious project is technically feasible.

6. Conclusion. Summary and outlook

It follows from the above that telescopes with focusing diffractive optics may be used efficiently in a wide range of energies (from EUV to soft gamma radiation) to study both thermal and nonthermal processes in the Universe.

Specifically, normal incidence telescopes may provide a fine angular resolution ($\sim 0.1''$) and an energy resolution sufficient to isolate a specific spectral line in the „densely populated“ EUV range. It appears promising to extend the applicability of such telescopes to the soft X-ray range.

The hard X-ray radiation range is presently covered fairly well by Wolter mirrors with wide-band multilayer gradient structures. The development of new and more efficient multilayer films and the application of active optics to compensate for the imperfect shape of mirrors (both at test stands and in orbit) are the probable objectives for research in the near-term future.

The high efficiency of focusing of soft gamma radiation by a Laue lens is key to its application in astrophysical studies. However, the current technology is still insufficient to construct optics to be mounted on a satellite. Innovative methods for fabrication of optical elements, such as quasi-mosaic crystals, and for assembly and precision alignment of a lens need to be developed.

The diffractive optics of Fresnel zone plates operates in a wide spectral interval (from soft X-ray to soft gamma radiation) and expands the capabilities of astrophysical instruments. Although it has several drawbacks, such as inconvenient focal distances and limited field of view and transmittance, its potential for concentration of a photon flux (specifically, the potential to achieve an excellent angular resolution) indicates that it should eventually find its place among the techniques used in celestial observations. However, this requires certain steps toward expanding the capabilities of focusing optics to be taken: the methods for fabrication of Fresnel zone plates with a parabolic zone profile and adjustable achromatic doublets need to be refined, and multiband (segmented) optics variants should be developed, produced, and aligned.

In view of the rapid progress in focusing diffractive optics, there is a chance that a telescope with a historically unparalleled angular resolution and its optics and receiving modules mounted on two satellites will be launched into orbit in the foreseeable future.

Funding

This study was supported by the Ministry of Science and Higher Education under the state assignment of the Shubnikov Institute of Crystallography „Crystallography and Photonics,“ Russian Academy of Sciences.

References

[1] K.P. Singh. J. Opt., **40** (3), 88 (2011). DOI: 10.1007/s12596-011-0040-2
[2] A.V. Vinogradov, B.Ya. Zel'dovich. Opt. Spektrosk., **42** (4), 708 (1977) (in Russian).
[3] E. Spiller. Experimental Methods Phys. Sci., **31**, 271 (1998). DOI: 10.1016/S0076-695X(08)60048-4
[4] F.E. Christensen, K.D. Joensen, P. Gorenstein, W.C. Priedhorsky, N.J. Westergaard, H.W. Schnopper. Exp. Astron., **6**, 33 (1995). DOI: 10.1007/BF00419256
[5] N. Lund. Exp. Astron., **2**, 259 (1992). DOI: 10.1007/BF00690085
[6] V.V. Lider. J. Surf. Invest.: X-Ray, Synchrotron Neutron Tech., **11** (6), 1113 (2017). DOI: 10.7868/S0207352817110026 [V.V. Lider. J. Surf. Invest. X-Ray Synchrotron Neutron Tech., **11**, 1113 (2017). DOI: 10.1134/S1027451017060155].
[7] A.G. Michette. *Optical systems for soft X-rays* (London, England. Plenum Press — New York and London, 1986).
[8] A.V. Vinogradov, I.A. Brytov, F.Ya. Grudskii. *Zerkal?naya rentgenovskaya optika*, Ed. A.V. Vinogradov (Mashinostroenie, L., 1989) (in Russian).
[9] T.W. Barbee. Opt. Eng., **25**, 898 (1986). DOI: 10.1117/12.949647
[10] M.P. Bruijn, J. Verhoeven, E.J. Puik, M.J. van der Wiel. Pros. SPIE, **984**, 54 (1988). DOI: 10.1117/12.948770
[11] M.M. Barysheva, A.E. Pestov, N.N. Salashchenko, M.N. Toropov, N.I. Chkhalo. Phys. Usp., **55** (7), 681 (2012). DOI: 10.3367/UFNr.0182.201207c.0727.
[12] Q. Huang, V. Medvedev, R. Wilhelmus E. van de Kruijs, A. Yakshin, E. Louis, F. Bijkerk. Appl. Phys. Rev., **4** (1), 011104 (2017). DOI: 10.1063/1.4978290
[13] I.V. Kozhevnikov, A.V. Vinogradov. Phys. Scr., **T17**, 137 (1987). DOI: 10.1088/0031-8949/1987/T17/015
[14] J.H. Underwood, T.W. Barbee. Appl. Opt., **20** (17), 3027-3034 (1981). DOI: 10.1364/AO.20.003027
[15] D.L. Windt. Computers in Phys., **12** (4), 360 (1998). DOI: 10.1063/1.168689
[16] D. Spiga, A. Mirone, C. Ferrero et al. Proc. SPIE, **5536**, 71 (2004).

[17] D. Spiga, A. Mirone, C. Ferrero, V. Cotroneo, G. Pareschi, M. Sanchez del Rio, D. Vernani. Proc. SPIE, **6266**, 626616 (2006). DOI: 10.1117/12.583232
[18] V.N. Oraevskii, I.I. Sobel′man, I.A. Zhitnik, V.D. Kuznetsov. Phys. Usp., **45** (8), 886 (2002). DOI: 10.3367/UFNr.0172.200208g.0949.
[19] S.V. Kuzin, V.N. Polkovnikov, N.N. Salashchenko. Bull. Russ. Acad. Sci. Phys., **75**, 84 (2011). DOI: 10.3103/S1062873811010151.
[20] D.G. Stearns, R.S. Rosen, S.P. Vernon. Opt. Lett., **16** (16), 1283 (1991). DOI: 10.1364/OL.16.001283
[21] B. Kjornrattanawanich, S. Bajt. Appl Opt., **43** (32), 5955 (2004). DOI: 10.1364/AO.43.005955
[22] C. Montcalm, B.T. Sullivan, M. Ranger, J.M. Slaughter, P.A. Kearney, C.M. Falco, M. Chaker. Opt. Lett., **19** (13), 1173 (1994). DOI: 10.1364/ol.19.001173
[23] C. Montcalm, B.T. Sullivan, S. Duguay, M. Ranger, W. Steffens, H. Pépin, M. Chaker. Opt. Lett., **20** (12), 1450 (1995). DOI: 10.1364/OL.20.001450
[24] A.J. Corso, P. Zuppella, D.L. Windt, M. Zangrando, M.G. Pelizzo. Opt. Express, **20** (7), 8006 (2012). DOI: 10.1364/OE.20.008006
[25] D.L. Windt, E.M. Gullikson. Appl. Opt., **54** (18), 5850 (2015). DOI: 10.1364/AO.54.005850
[26] D.L. Windt. Proc. SPIE, **9604**, 96040P (2015). DOI: 10.1117/12.2188230
[27] N.I. Chkhalo, S. Künstner, V.N. Polkovnikov, N.N. Salashchenko, F. Schäfers, S.D. Starikov. Appl. Phys. Lett., **102**, 011602 (2013). DOI: 10.1063/1.4774298
[28] M. Suman, M.G. Pelizzo, D.L.Windt, P. Nicolosi. Appl. Opt., **48** (29), 5432 (2009). DOI: 10.1364/AO.48.005432
[29] Z.S. Wang, H.C. Wang, J.T. Zhu, F. Wang, Z. Gu, L. Chen, A.G. Michette, A.K. Powell, S.J. Pfauntsch, F. Schäfers. Opt. Express, **14** (6), 2533(2006). DOI: 10.1364/OE.14.002533
[30] H.C. Wang, J.T. Zhu, Z.S. Wang, Z. Zhang, S.Zhang, W. Wu, L. Chen, A.G. Michette, A.K. Powell, S.J. Pfauntsch, F. Schäfers, A. Gaupp. Thin Solid Films, **515** (4), 2523 (2006). DOI: 10.1016/j.tsf.2006.04.039
[31] D.G. Stearns, R.S. Rosen, S.P. Vernon. J. Vac. Sci. Technol., **A 9** (5), 2662 (1991). DOI: 10.1116/1.577221
[32] S. Bajt, J.B. Alameda, T.W. Barbee Jr., W.M. Clift, J.A. Folta, B. Kaufmann, E.A. Spiller. Opt. Eng., **41** (8), 1797 (2002). DOI: 10.1117/1.1489426
[33] N. Chkhalo, S. Gusev, A. Nechay, D. Pariev, V. Polkovnikov, N. Salashchenko, F. Schäfers, M. Sertsu, A. Sokolov, M. Svechnikov, D. Tatarsky. Opt. Lett., **42** (24), 5070 (2017). DOI: 10.1364/OL.42.005070
[34] S.S. Andreev, S.V. Gaponov, S.A. Gusev. Thin Solid Films, **415** (1–2), 123 (2002). DOI: 10.1016/S0040-6090(02)00536-9
[35] J. Zhu, D. Xu, S. Zhang, H. Wang, W. Wu, B. Wang, Y. Xu, Z. Zhang, F. Wang, L. Chen, H. Zhou, T. Huo. Front. Optoelectron. China, **1**, 305, (2008). DOI: 10.1007/s12200-008-0028-y
[36] E. Meltchakov, C. Hecquet, M. Roulliay, S.D. Rossi, Y. Menesguen, A. Jérome, F. Bridou, F. Varniere, M.-F. Ravet-Krill, F. Delmottel. Appl. Phys. A, **98** (1),111 (2010). DOI: 10.1007/s00339-009-5445-2
[37] D.L. Windt, J.A. Bellotti. Appl. Optics, **48** (26), 4932 (2009). DOI: 10.1364/AO.48.004932.
[38] M-H. Hu, K. Le Guen, J.-M. André, P. Jonnard, E. Meltchakov, F. Delmotte, A. Galtayries. Opt. Express, **18** (19), 20019 (2010). DOI: 10.1364/OE.18.020019
[39] S.Yu. Zuev, S.V. Kuzin, V.N. Polkovnikov, N.N. Salashchenko. Bull. Russ. Acad. Sci. Phys., **74**, 50 (2010). DOI: 10.3103/S1062873810010132.
[40] Q. Zhong, Z. Zhang, W. Li, J. Zhu, Z. Wang, P. Jonnard, K. Le Guen, Y. Yuan, J.-M. André, H. Zhou, T. Huo. J. Phys.: Conf. Ser., **425** (15), 152010 (2013). DOI: 10.1088/1742-6596/425/15/152010
[41] N.I. Chkhalo, D.E. Pariev, V.N. Polkovnikov, N.N. Salashchenko, R.A. Shaposhnikov, I.L. Stroulea, M.V. Svechnikov, Yu.A. Vainer, S.Yu. Zuev. Thin Solid Films, **631**, 106 (2017). DOI: 10.1016/j.tsf.2017.04.020
[42] J. Zhu, S. Zhou, H. Li, Q. Huang, L. Jiang, F. Wang, Z. Zhang, Z. Wang, H. Zhou, T. Huo. Proc. SPIE, **8168** 81681C (2012). DOI: 10.1117/12.896405
[43] J. Zhu, S. Zhou, H. Li, Q. Huang, Z.S. Wang, K. Le Guen, M-H. Hu, J.-M. André, P. Jonnard. Appl. Opt., **49** (20), 3922–3925 (2010). DOI: 10.1364/AO.49.003922
[44] I. Yoshikawa, T. Murachi, H. Takenaka, S. Ichimaru. Rev. Sci. Inst., **76** (6), 066109 (2005). DOI: 10.1063/1.1938867
[45] H. Takenaka, S. Ichimaru, T. Ohchi, E.M. Gullikson. J. Electron Spec. Rel. Phen. **144–147**, 1047 (2005). DOI: 10.1016/j.elspec.2005.01.227
[46] R. Soufli, D.L. Windt, J.C. Robinson, S.L. Baker, E. Spiller, F.J. Dollar, A.L. Aquila, E.M. Gullikson, B. Kjornrattanawanich, J.F. Seely, L. Golub. Proc. SPIE, **5901** 59010M (2005). DOI: 10.1117/12.617370
[47] H. Maury, P. Jonnard, K. Le Guen, J.-M. André, Z. Wang, J. Zhu, J. Dong, Z. Zhang, F. Bridou, F. Delmotte, C. Hecquet, N. Mahne, A. Giglia, S. Nannarone. Eur. Phys. J., **B 64** (2), 193 (2008). DOI: 10.1140/epjb/e2008-00290-x
[48] R. Soufli, M. Fernández-Perea, J.C. Robinson, S.L. Baker, J. Alameda, E.M. Gullikson. Proc. SPIE, **8443**, 84433R (2012). DOI: 10.1117/12.926589
[49] S.A. Bogachev, N.I. Chkhalo, S.V. Kuzin, D.E. Pariev, V.N. Polkovnikov, N.N. Salashchenko, S.V. Shestov, S.Y. Zuev. Appl. Optics, **55** (9), 2126 (2016). DOI: 10.1364/AO.55.002126
[50] H.C. Li, S.K. Zhou, X. Wang., J. Zhu, Z.Wang. Proc. SPIE, **8501**, 85010G (2012). DOI: 10.1117/12.929448
[51] K. Le Guen, M.-H. Hu, J.-M. André, P. Jonnard, S.-K. Zhou, H.-C. Li, J.-T. Zhu, Z.-S. Wang, C. Meny. J. Phys. Chem. C, **114** (14), 6484 (2010). DOI: 10.1021/jp911119z
[52] H. Li, J. Zhu, S. Zhou. Appl. Phys. Lett., **102** (11), 111103 (2013). DOI: 10.1063/1.4794399
[53] D.L. Windt, S. Donguy, J.F. Seely, B. Kjornrattanawanich. Appl. Opt., **43** (9), 1835 (2004). DOI: 10.1364/ao.43.001835.
[54] V.N. Polkovnikov, N.I. Chkhalo, R.S. Pleshkov, N.N. Salashchenko, F. Schäfers, M.G. Sertsu, A. Sokolov, M.V. Svechnikov, S.Yu. Zuev. Opt. Lett., **44** (2), 263 (2019). DOI: 10.1364/OL.44.000263
[55] Yu.A. Uspenskii, V.E. Levashov, A.V. Vinogradov, A.I. Fedorenko, V.V. Kondratenko, Yu.P. Pershin, E.N. Zubarev, S. Mrowka, F. Schäfers. Nucl. Instr. and Meth. A, **448** (1–2), 147 (2000). DOI: 10.1016/S0168- 9002(00)00212-6
[56] Yu.A. Uspenskii, S.V. Antonov, V.Yu. Fedotov, A.V. Vinogradov. Proc. SPIE, **3156**, 288 (1997). DOI: 10.1117/12.279412
[57] A.V. Vinogradov. Quantum Electron., **32** (12), 1113 (2002).

[58] D.L. Windt, S. Donguy, J. Seely, B. Kjornrattanawanich, E.M. Gullikson, C.C. Walton, L. Golub, E. DeLuca. Proc. SPIE, **5168**, 1 (2003). DOI: 10.1117/12.506175
[59] F. Schäfers, S. Yulin, T. Feigl, N. Kaiser. Proc. SPIE, **5188**, 138 (2003). DOI: 10.1117/12.505695
[60] Y.A. Uspenskii, V.E. Levashov, A.V. Vinogradov, A.I. Fedorenko, V.V. Kondratenko, Yu.P. Pershin, E.N. Zubarev, V.Yu. Fedotov. Opt. Lett., **23** (10), 771 (1998). DOI: 10.1364/OL.23.000771
[61] M. Fernández-Perea, R. Soufli, J.C. Robinson, L. Rodríguez-De Marcos, J.A. Méndez, J.I. Larruquert, E.M. Gullikson. Opt. Express, **20** (21), 24018 (2012). DOI: 10.1364/OE.20.024018
[62] S.V. Kuzin, I.A. Zhitnik, S.V. Shestov, S.A. Bogachev, O.I. Bugaenko, A.P. Ignat'ev, A.A. Pertsov, A.S. Ulyanov, A.A. Reva, V.A. Slemzin, N.K. Sukhodrev, Yu.S. Ivanov, L.A. Goncharov, A.V. Mitrofanov, S.G. Popov, T.A. Shergina, V.A. Solov'ev, S.N. Oparin, A.M. Zykov. Sol. Syst. Res., **45** (2), 162 (2011). DOI: 10.1134/S0038094611020110.
[63] B. Kjornrattanawanich, D.L. Windt, J.F. Seely. Opt. Lett., **33** (9), 965 (2008). DOI: 10.1364/OL.33.000965
[64] M. Vidal-Dasilva, M. Fernández-Perea, J.I. Larruquert. Proc. SPIE, **7448**, 74480N (2009). DOI: 10.1117/12.827969
[65] D.L. Windt, J.F. Seely, B. Kjornrattanawanich, Yu.A. Uspenskii. Opt. Lett., **30** (23), 3186 (2005). DOI: 10.1364/OL.30.003186
[66] B. Kjornrattanawanich, D.L. Windt, J.F. Seely, Y.A. Uspenskii. Appl. Opt., **45** (8), 1765 (2006). DOI: 10.1364/AO.45.001765
[67] B. Kjornrattanawanich, D.L. Windt, Yu.A. Uspenskii, J.F. Seely. Proc. SPIE, **6317**, 63170U (2006). DOI: 10.1117/12.681952
[68] J.F. Seely, Yu.A. Uspenskii, B. Kjornrattanawanich, D.L. Windt. Proc. SPIE, **6317**, 63170T (2006). DOI: 10.1117/12.683234
[69] N. Chkhalo, V. Polkovnikov, N. Salashchenko, M. Svechnikov, N. Tsybin, Y. Vainer, S. Zuev. Opt. Lett., **45** (17), 4666 (2020). DOI: 10.1364/OL.400526
[70] U. Schühle, J.-P. Halain, S. Meining, L. Teriaca. Proc. SPIE, **8148**, 81480K (2011). DOI: 10.1117/12.893573
[71] P. Rochus, J.-M. Defise, J.-P. Halain, C. Jamar, E. Mazy, L. Rossi, T. Thibert, F. Clette, P. Cugnon, D. Berghmans, J.-F. Hochedez, J.-P. Delaboudiniére, F. Auchére, R. Mercier, M.-F. Ravet, F. Delmotte, M. Idir, U. Schühle, V. Bothmer, S. Fineschi, R.A. Howard, J.D. Moses, J. Newmark. Proc. SPIE, **5171**, 53 (2004). DOI: 10.1117/12.503964
[72] J.P. Halain, A. Mazzoli, S. Meining, P. Rochus, E. Renotte, F. Auchére, U. Schühle, F. Delmotte, C. Dumesnil, A. Philippon, R. Mercier, A. Hermans. Proc. SPIE, **9604**, 96040H (2015). DOI: 10.1117/12.2185631
[73] A. Galtayries, M.-H. Hu, K. Le Guen, J.-M. André, P. Jonnard, E. Meltchakov, C. Hecquet, F. Delmotte. Surf. Interface Anal., **42** (6–7), 653 (2010). DOI: 10.1002/sia.3393
[74] H.-J. Voorma, E. Louis, F. Bijkerk, S. Abdali. J. Appl. Phys., **82** (4), 1876 (1997). DOI: 10.1063/1.365992
[75] T. Kuhlmann, S. Yulin, T. Feigl, N. Kaiser, T. Gorelik, U. Kaiser, W. Richter. Appl. Opt., **41** (10), 2048 (2002). DOI: 10.1364/AO.41.002048
[76] J. Birch, F. Eriksson, G.A. Johansson, H.M. Hertz. Vacuum, **68** (3), 275 (2003). DOI: 10.1016/S0042-207X(02)00457-8
[77] E. Louis, H.-J. Voorn, N.B. Koster, L. Shmacnok, F. Bijkcrk, R. Schlatmar, J. Verhoeven, Yu.Ya. Platonov, G.E. van Dorsscnd H.A. Padmorc. Microel. Engineering, **23** (1–4), 215 (1994). DOI: 10.1016/0167-9317(94)90140-6
[78] A. Guggenmos, S. Radünz, R. Rauhut, M. Hofstetter, S. Venkatesan, A. Wochnik, E.M. Gullikson, S. Fischer, B. Nickel, C. Scheu, U. Kleineberg. Opt. Express, **22** (22), 26526 (2014). DOI: 10.1364/OE.22.026526
[79] R. Soufli, S.L. Baker, E.M. Gullikson, T. Mc Carville, J.C. Robinson, D. Martínez-Galarce, M. Fernández-Perea, M.J. Pivovaroff. Proc. SPIE, **8501**, 850102 (2012). DOI: 10.1117/12.954852
[80] E.N. Zubarev, V.V. Kondratenko, V.A. Sevryukova, S.A. Yulin, T. Feigl, N. Kaiser. Appl. Phys. A, **90**, 705 (2008). DOI: 10.1007/s00339-007-4337-6
[81] A. Kloidt, K. Nolting, U. Kleineberg, B. Schmiedeskamp, U. Heinzmann. Appl. Phys. Lett., **58** (23), 2601 (1991). DOI: 10.1063/1.104835
[82] H.-J. Voorma, E. Louis, N.B. Koster, F. Bijkerk. J. Appl. Phys., **83** (9), 4700 (1998). DOI: 10.1063/1.367258
[83] M. Niibe, M. Hayashida, T. Iizuka, A. Miyake, Y. Watanabe, R. Takahashi, Y. Fukuda. Proc. SPIE, **1343**, 2 (1990). DOI: 10.1117/12.23172
[84] V.I.T.A. de Rooij-Lohmann, A.E. Yakshin, E. Zoethout, J. Verhoeven, F. Bijkerk. Appl. Surf. Science, **257**, (14), 6251 (2011). DOI: 10.1016/j.apsusc.2011.02.054
[85] J.A. Bellotti, D.L. Windt. Proc. SPIE, **7437**, 743715 (2009). DOI: 10.1117/12.824628
[86] D.L. Windt. Proc. SPIE, **6688**, 66880R (2007). DOI: 10.1117/12.730647
[87] D.L. Windt, W.L. Brown, C.A. Volkert, W.K. Waskiewicz. J. Appl. Phys., **78** (4), 2423 (1995). DOI: 10.1063/1.360164
[88] P.B. Mirkarimi, C. Montcalm. Proc. SPIE, **3331**, 133 (1998). DOI: 10.1117/12.309565
[89] Q. Yi, Q. Huang, X. Wang, Y. Yang, X. Yang, Z. Zhang, Z. Wang, R. Xu, T. Peng, H. Zhou, T. Huo. Appl Opt., **56** (4), C145 (2017). DOI: 10.1364/AO.56.00C145
[90] T. Feigl, S. Yulin, T. Kuhlmann, N. Kaiser. Proc SPIE, **4506**, 121 (2001). DOI: 10.1117/12.436715
[91] M.E. Kassner, F.J. Weber, J. Koike, R.S. Rosen. J. Mat. Sci., **31**, 2291 (1996). DOI: 10.1007/BF01152937
[92] M. Barthelmess, S. Bajt. Appl. Opt., **50** (11), 1610 (2011). DOI: 10.1364/AO.50.001610
[93] P.B. Mirkarimi. Opt. Eng., **38** (7), 1246 (1999). DOI: 10.1117/1.602170
[94] M. Shiraishi, W. Ishiyama, T. Ohsino, K. Murakami. Jpn. J. App. Phys., **39** (Part 1, № 12B), 6810 (2000). DOI: 10.1109/IMNC.2000.872766
[95] T. Leisegang, D.C. Meyer, A.A. Levin, S. Braun, P. Paufler. Appl. Phys. A, **77** (7), 965 (2003). DOI: 10.1007/s00339-003-2259-5
[96] D. Windt. Proc. SPIE, **3448**, 280 (1998). DOI: 10.1117/12.332515
[97] D.L. Windt. J. Vac. Sci. Tech. B, **17** (4), 1385 (1999). DOI: 10.1116/1.590841
[98] S.S. Andreev, N.N. Salashchenko, L.A. Suslov, A.N. Yablonsky, S.Y. Zuev. Nucl. Instr. and Meth. A, **470** (1), 162 (2001). DOI: 10.1016/S0168- 9002(01)01018-X
[99] S.V. Kuzin, A.A. Reva, S.A. Bogachev, N.F. Erkhova, N.N. Salashchenko, N.I. Chkhalo, V.N. Polkovnikov. Tech. Phys., **65** (11), 1736 (2020). DOI: 10.21883/JTF.2020.11.49967.113-20
[100] R.B. Hoover, P.C. Baker, J.B. Hadaway, R.B. Johnson, C. Peterson, D.R. Gabardi, A.B.C. Walker, Jr., J.F. Lindblom,

C. De Forest, R.H. O′Neal. Proc. SPIE, **1343**, 189 (1991). DOI: 10.1117/12.23192
[101] V.A. Slemzin, I.A. Zhitnik, E.N. Ragozin, E.A. Andreev, N.N. Salashchenko, J.Y. Platonov. Proc. SPIE, **2279**, 234 (1994). DOI: 10.1117/12.193140
[102] A.B.C. Walker Jr., J.F. Lindblom, R.H. O′Neal, V.J. Allen, T. Barbee, R. Hoover. Opt. Eng., **29** (6), 581 (1990). DOI: 10.1117/12.55640
[103] A.B.C. Walker, M.J. Allen Jr., C.E. De Forest, C.C. Kankelborg, Martinez- D.S. Galarce, J.E. Plummer, R.B. Hoover, T.W. Barbee Jr, D.B. Gore. Proc. SPIE, **2515**, 182 (1995). DOI: 10.1117/12.212587
[104] D.S. Martínez-Galarce, A.B.C. Walker, D.B. Gore, C.C. Kankelborg, R.B. Hoover, T.W. Barbee Jr., P.F.X. Boerner. Opt. Eng., **39** (4), 1063 (2000). DOI: 10.1117/1.602468
[105] B.N. Handy, L.W. Acton, C.C. Kankelborg, C.J. Wolfson, D.J. Akin, M.E. Bruner, R. Caravalho, R.C. Catura, R. Chevalier, D.W. Duncan, C.G. Edwards, C.N. Feinstein, S.L. Freeland, F.M. Friedlaender, C.H. Hoffmann, N.E. Hurlburt, B.K. Jurcevich, N.L. Katz, G.A. Kelly, J.R. Lemen, M. Levay, R.W. Lindgren, D.P. Mathur, S.B. Meyer, S.J. M.D. Morrison, Morrison, R.W. Nightingale, T.P. Pope, R.A. Rehse, C.J. Schrijver, R.A. Shine, L. Shing, K.T. Strong, T.D. Tarbell, A.M. Title, D.D. Torgerson, L. Golub, J.A. Bookbinder, D. Caldwell, P.N. Cheimets, W.N. Davis, E.E. Deluca, R.A. Mc Mullen, H.P. Warren, D. Amato, R. Fisher, H. Maldonado, C. Parkinson. Sol. Phys., **187**, 229 (1999). DOI: 10.1023/A:1005166902804
[106] H.P. Warren. Stars as Suns: Activity, Evolution, and Planets IAU Symposium, **219**, 91 (2004)
[107] D.S. Martinez-Galarce, P. Boerner, R. Soufli, B. De Pontieu, N. Katz, A. Title, E.M. Gullikson, J.C. Robinson, S.L. Baker. Proc. SPIE, **7011**, 70113K (2008). DOI: 10.1117/12.788508
[108] K. Kobayashi, H. Hara, R. Kano, S. Nagata, T. Sakao, T. Shimizu, S. Tsuneta, T. Yoshida, R.A. Harrison. Publ. Astron. Soc. Japan, **52**, 1165 (2000). DOI: 10.1093/pasj/52.6.1165
[109] P. Boerner, C. Edwards, J. Lemen, A. Rausch, C. Schrijver, R. Shine, L. Shing, R. Stern, T. Tarbell, A. Title, C.J. Wolfson, R. Soufli, E. Spiller, E. Gullikson, D. McKenzie, D. Windt, L. Golub, W. Podgorski, P. Testa, M. Weber. Solar Phys., **275** (1–2), 41 (2012). DOI: 10.1007/s11207-011-9804-8
[110] D.S. Martínez-Galarce, R. Soufli, D.L., M. Windt Bruner, E. Gullikson, S. Khatri, E. Spiller, J.C. Robinson, S. Baker, E. Prast. Opt. Eng., D.L., **52** (9), 095102 (2013). DOI: 10.1117/1.OE.52.9.095102
[111] J.P. Delaboudiniére, G.E. Artzner, J. Brunaud, A.H. Gabriel, J.F. Hochedez, F. Millier, X.Y. Song, B. Au, K.P. Dere, R.A. Howard, R. Kreplin, D.J. Michels, J.D. Moses, J. Defise, C. Jamar, P. Rochus, J.P. Chauvineau, J.P. Marioge, R.C. Catura, J.R. Lemen, L. Shing, R.A. Stern, J.B. Gurman, W.M. Neupert, A. Maucherat, F. Clette, P. Cugnon, E.L. Van Dessel. Sol. Phys., **162** (1), 291 (1995). DOI: 10.1007/BF00733432
[112] J.-P. Wülser, J.R. Lemen, T.D. Tarbell, C.J. Wolfson, J.C. Cannon, B.A. Carpenter, D.W. Duncan, G.S. Gradwohl, S.B. Meyer, A.S. Moore, R.L. Navarro, J.D. Pearson, G.R. Rossi, L.A. Springer, R.A. Howard, J.D. Moses, J.S. Newmark, J.-P. Delaboudiniére, G. Artzner, F. Auchére, M. Bougnet, P. Bouyries, F. Bridou, J.-Y. Clotaire, G. Colas, F. Delmotte, A. Jerome, M. Lamare, R. Mercier, M. Mullot, M.-F. Ravet, X. Song, V. Bothmer, W. Deutsch. Proc. SPIE, **5171**, 111 (2004). DOI: 10.1117/12.506877
[113] V. Slemzin, O. Bougaenko, A. Ignatiev, S. Kuzin, A. Mitrofanov, A. Pertsov, I. Zhitnik. Ann. Geophys., **26** (10), 3007 (2008). DOI: 10.5194/angeo- 26-3007-2008
[114] V.A. Slemzin, S.V. Kuzin, I.A. Zhitnik, J.-P. Delaboudiniere, F. Auchere, A.N. Zhukov, R. Van der Linden, O.I. Bugaenko, A.P. Ignat′ev, A.V. Mitrofanov, A.A. Pertsov, S.N. Oparin, A.I. Stepanov, A.N. Afanas′ev. Solar Syst. Res., **39**, 489 (2005). DOI: 10.1007/s11208-005-0062-x.
[115] A.C. Katsiyannis, D. Berghmans, J.-F. Hochedez, B. Nicula, G. Lawrence, J.-M. Defise, A. Ben-Moussa, V. Delouille, M. Dominique, J.-H. Lecat, W. Schmutz, A. Theissen, V. Slemzin. Proc. SPIE, **5901**, 59010V (2005). DOI: 10.1117/12.616803
[116] D.B. Seaton, D. Berghmans, B. Nicula, J.-P. Halain, A. De Groof, T. Thibert, D.S. Bloomfield, C.L. Raftery, P.T. Gallagher, F. Auchére, J.-M. Defise, E. D'Huys, J.-H. Lecat, E. Mazy, P. Rochus, L. Rossi, U. Schühle, V. Slemzin, M.S. Yalim, J. Zender. Solar Phys., **286** (1), 43 (2013). DOI: 10.1007/s11207-012-0114-6
[117] S.A. Bogachev, S.V. Kuzin, A.A. Pertsov, S.V. Shestov, Yu.S. Ivanov, A.S. Ul'yanov, A.S. Kirichenko, A.A. Reva. Mekh., Upr. Inf., **2** (14), 5 (2013) (in Russian).
[118] S.V. Kuzin, S.A. Bogachev, A.A. Pertsov, S.V. Shestov, A.A. Reva, A.S. Ulyanov. Bull. Russ. Acad. Sci. Phys., **75** (1), 87 (2011). DOI: 10.3103/S1062873811010163.
[119] S.V. Kuzin, S.A. Bogachev, I.A. Zhitnik, S.V. Shestov, V.A. Slemzin, A.V. Mitrofanov, N.K. Sukhodrev, A.A. Pertsov, A.P. Ignatiev, O.I. Bugaenko, Yu.S. Ivanov, A.A. Reva, M.S. Zykov, A.S. Ulyanov, S.N. Oparin, A.L. Goncharov, T.A. Shergina, A.M. Urnov, V.A. Soloviev, S.G. Popova. Bull. Russ. Acad. Sci.: Phys., **74** (1), 33 (2010). DOI: 10.3103/S1062873810010090.
[120] L.A. Rachmeler, A.R. Winebarger, S.L. Savage, L. Golub, K. Kobayashi, G.D. Vigil, D.H. Brooks, J.W. Cirtain, B. D Pontieu, D.E. Mc Kenzie, R.J. Morton, H. Peter, P. Testa, S.K.Tiwari, R.W. Walsh, H.P. Warren, C. Alexander, D. Anse, B.L. Beabout, D.L. Beabout, C.W. Bethge, P.R. Champey, P.N. Cheimets, M.A. Cooper, H.K. Cree, R. Gates, C. Gomez, A. Guillory, H. Haight, W.D. Hogue, T. Holloway, D.W. Hyde, R. Kenyon, J.N. Marshall, E. McCracken, K. McCracken, K.O. Mitchel, M. Ordway, T. Owen, J. Ranganathan, B.A. Robertson, M.J. Payne, W. Podgorski, J. Pryor, J. Samra, M.D. Sloan, H.A. Soohoo, D.B. Steele, F.V. Thompson, G.S. Thornton, B. Watkinson, D. Windt. Sol. Phys., **294** (12), 174 (2019). DOI: 10.1007/s11207-019-1551-2
[121] J.-P. Halain, Y. Houbrechts, F. Auchére. Proc. SPIE, **10565**, 1056561 (2010). DOI: 10.1117/12.2552542
[122] P. Rochus, F. Auchére, D. Berghmans, L. Harra, W. Schmutz, U. Schühle, P. Addison, T. Appourchaux, R. Aznar Cuadrado, D. Baker, J. Barbay, D. Bates, A. BenMoussa, M. Bergmann, C. Beurthe, B. Borgo, K. Bonte, M. Bouzit, L. Bradley, V. Bchel, E. Buchlin, J. Bchner, F. Cabé, L. Cadiergues, M. Chaigneau, B. Chares, C. Choque Cortez, P. Coker, M. Condamin, S. Coumar, W. Curdt, J. Cutler, D. Davies, G. Davison, J.-M. Defise, G. Del Zanna, F. Delmotte, V. Delouille, L. Dolla, C. Dumesnil, F. Dürig, R. Enge, S. François, J.-J. Fourmond, J.-M. Gillis, B. Giordanengo, S. Gissot, L. M. Green, N. Guerreiro, A. Guilbaud, M. Gyo,

M. Haberreiter, A. Hafiz, M. Hailey, J.-P. Halain, J. Hansotte, C. Hecquet, K. Heerlein, M.-L. Hellin, S. Hemsley, A. Hermans, V. Hervier, J.-F. Hochedez, Y. Houbrechts, K. Ihsan, L. Jacques, A. Jérôme, J. Jones, M. Kahle, T. Kennedy, M. Klaproth, M. Kolleck, S. Koller, E. Kotsialos, E. Kraaikamp, P. Langer, A. Lawrenson, J.-C. Le Clech', C. Lenaerts, S. Liebecq, D. Linder, D. M. Long, B. Mampaey, D. Markiewicz-Innes, B. Marquet, E. Marsch, S. Matthews, E. Mazy, A. Mazzoli, S. Meining, E. Meltchakov, R. Mercier, S. Meyer, M. Monecke, F. Monfort, G. Morinaud, F. Moron, L. Mountney, R. Múller, B. Nicula, S. Parenti, H. Peter, D. Pfiffner, A. Philippon, I. Phillips, J.-Y. Plesseria, E. Pylyser, F. Rabecki, M.-F. Ravet-Krill, J. Rebellato, E. Renotte, L. Rodriguez, S. Roose, J. Rosin, L. Rossi, P. Roth, F. Rouesnel, M. Roulliay, A. Rousseau, K. Ruane, J. Scanlan, P. Schlatter, D. B. Seaton, K. Silliman, S. Smit, P. J. Smith, S.K. Solanki, M. Spescha, A. Spencer, K. Stegen, Y. Stockman, N. Szwec, C. Tamiatto, J. Tandy, L. Teriaca, C. Theobald, I. Tychon, L. van Driel-Gesztelyi, C. Verbeeck, J.-C. Vial, S. Werner, M.J. West, D. Westwood, T. Wiegelmann, G. Willis, B. Winter, A. Zerr, X. Zhang, A.N. Zhukov. Astron. Astrophys., **642**, A8 (2020). DOI: 10.1051/0004-6361/201936663

[123] C. Hecquet, F. Delmotte, M.-F. Ravet-Krill, S. de Rossi, A. Jérome, F. Bridou, F. Varniére, E. Meltchakov, F. Auchére, A. Giglia, N. Mahne, S. Nanaronne. Appl. Phys., **A 95** (2), 401 (2009). DOI: 10.1007/s00339-009- 5082-9

[124] D.L. Windt, S.M. Kahn. Proc. SPIE, **4851**, 441 (2003). DOI: 10.1117/12.461288

[125] K.D. Joensen, P. Voutov, A. Szentgyorgyi, J. Roll, P. Gorenstein, P. Høghøj, F.E. Christensen. Appl. Opt., **34** (34), 7935 (1995). DOI: 10.1364/AO.34.007935

[126] P.H. Mao, F.A. Harrison, D.L. Windt, F.E. Christensen. Appl. Opt., **38** (22), 4766 (1999). DOI: 10.1364/ao.38.004766

[127] A.V. Vinogradov, R.M. Faschenko. Nucl. Instrum. Methods Phys. Res. A, **448** (1), 142 (2000). DOI: 10.1016/S0168-9002(99)00723-8

[128] I.V. Kozhevnikov, I.N. Bukreeva, E. Ziegler. Design of X-ray supermirrors. Nucl. Instrum. Methods Phys. Res. A, **460** (2−3), 424 (2001). DOI: 10.1016/S0168-9002(00)01079-2

[129] Ch. Morawe, E. Ziegler, J.Ch. Peffen, I.V. Kozhevnikov. Nucl. Instrum. Methods Phys. Res. A, **493** (3), 189 (2002). DOI: 10.1016/S0168- 9002(02)01570-X

[130] D.L. Windt. Proc. SPIE, **9603**, 96031C (2015). DOI: 10.1117/12.2187481

[131] D. Spiga. Extraction of Multilayer Coating Parameters from X-Ray Reflectivity Data. In: *Modern Developments in X-Ray and Neutron Optics* (A. Erko, M. Idir, T. Krist, A.G. Michette (Eds.) Springer-Verlag, Berlin, Heidelberg, 2008), p. 233. DOI: 10.1007/978-3-540-74561-7_16

[132] K. Yamashita, P.J. Serlemitsos, J. Tueller, S.D. Barthelmy, L.M. Bartlett, K.-W. Chan, A. Furuzawa, N. Gehrels, K. Haga, H. Kunieda, P. Kurczynski, G. Lodha, N. Nakajo, N. Nakamura, Y. Namba, Y. Ogasaka, T. Okajima, D. Palmer, A. Parsons, Y. Soong, C.M. Stahl, H. Takata, K. Tamura, Y. Tawara, B.J. Teegarden. Appl. Opt., **37** (34), 8067 (1998). DOI: 10.1364/ao.37.008067

[133] Y. Tawara, K. Yamashita, H. Kunieda, K. Tamura, A. Furuzawa, K. Haga, N. Nakajo, T. Okajima, H. Takata, P.J. Serlemitsos, J. Tueller, R. Petre, S. Yang, K.W. Chan, G.S. Lodha, Y. Namba, J. Yu. SPIE Proc., **3444**, 569 (1998). DOI: 10.1117/12.331278

[134] K. Madsen, F.A. Harrison, P.H. Mao, F.E. Christensen, P. Carsten, J. Brejnholt, N. Brejnholt, J. Koglin, M.J. Pivovaroff. Proc. SPIE, **7437**, 743716 (2009). DOI: 10.1117/12.826669

[135] D.L. Windt. Appl. Phys. Lett., **74** (19), 2890 (1999). DOI: 10.1063/1.124048

[136] F.E. Christensen, C.P. Jensen, K.K. Madsen, M.J. Pivovaroff, H. Chen, A. Dariel, P. Høghøj. Proc. SPIE, **6266**, 28 (2006). DOI: 10.1117/12.673181

[137] C.P. Jensen, K.K. Madsen, F.E. Christensen. Exp. Astron., **20** (1−3), 93 (2005). DOI: 10.1007/978-1-4020-5304-7_11

[138] C.P. Jensen, K.K. Madsen, F.E. Christensen. Proc. SPIE, **6266**, 626612 (2006). DOI: 10.1117/12.673180

[139] T. Okajima, K. Tamura, Y. Ogasaka, K. Haga, S. Takahashi, S. Ichimaru, H. Kito, S. Fukuda, A. Goto, K. Nomoto, H. Satake, S. Kato, Y. Kamata, A. Furuzawa, F. Akimoto, T. Yoshioka, K. Kondo, Y. Haba, T. Tanaka, K. Wada, N. Hamada, M. Hudaverdi, Y. Tawara, K. Yamashita, P.J. Serlemitsos, Y. Soong, K.-W. Chan, S.M. Owens, F.B. Berendse, J. Tueller, K. Misaki, R. Shibata, H. Mori, K. Itoh, H. Kunieda, Y. Namba. Appl. Opt., **41** (25), 5417 (2002). DOI: 10.1364/ao.41.005417

[140] Y. Ogasaka, J. Tueller, K. Yamashita, P. Serlemitsos, R. Shibata, K. Tamura, A. Furuzawa, T. Miyazawa, R. Takahashi, M. Sakashita, K. Shimoda, Y. Tawara, H. Kunieda, T. Okajima, H. Krimm, S. Barthelmy, Y. Soong, K.W. Chan, S. Owens, M. Rex, E. Chapin, M. Devlin. Proc. SPIE, **5900**, 59000R (2005). DOI: 10.1117/12.616677

[141] J. Tueller, H.A. Krimm, T. Okajima, S.D. Barthelmy, S.M. Owens, P.J. Serlemitsos, Y. Soong, K.-W. Chan, Y. Ogasaka, R. Shibata, K. Tamura, A. Furuzawa, Y. Tawara, H. Kunieda, K. Yamashita. Exp. Astron., **20** (1), 121 (2005). DOI: 10.1007/978-1-4020-5304-7_14

[142] H. Wolter. Ann. Phys. **10**, 94 (1952). DOI: 10.1002/andp.19524450108

[143] P. Gorenstein. X-Ray Opt. Instrum., **2010** (1−2), ID 109740 (2010). DOI: 10.1155/2010/109740

[143] R. Petre, P.J. Serlemitsos. Appl. Opt., **24** (12), 1833 (1985). DOI: 10.1364/AO.24.001833

[144] C.J. Hailey, S. Abdali, F.E. Christensen, W.W. Craig, T.R. Decker, F.A. Harrison, M.A. Jimenez-Garate. Proc. SPIE, **3114**, 535 (1997). DOI: 10.1117/12.278902

[145] W.W. Craig, F.E. Christensen, T.A. Decker, C.J. Hailey, F.A. Harrison, R.M. Hul, M. Jimenez-Garate, P. Mao, S. Schindler. Proc. SPIE, **3445**, 112 (1998). DOI: 10.1117/12.330269

[146] W.W. Craig, C.J. Hailey, M. Jimenez-Garate, D.L. Windt. Opt. Express, **7** (4), 178 (2000). DOI: 10.1364/OE.7.000178

[147] F.A. Harrison, S.E. Boggs, A. Bolotnikov, F.E. Christensen, W.R. Cook, W.W. Craig, C.J. Hailey, M. Jimenez-Garate, P.H. Mao, S.E. Schindler, D.L. Windt. Proc. SPIE, **4012**, 693 (2000). DOI: 10.1117/12.391608

[148] J.E. Koglin, F.E. Christensen, J. Chonko, W.W. Craig, T.R. Decker, M.A. Jimenez-Garate, K. Gunderson, C.J. Hailey, F.A. Harrison, C.P. Jensen, M. Sileo, D.L. Windt, H. Yu. Proc. SPIE, **4851**, 607 (2003). DOI: 10.1117/12.461479

[149] C.P. Jensen, K.K. Madsen, H.C. Chen, E. Ziegler. Proc. SPIE, **4851**, 724 (2003). DOI: 10.1117/12.461315

[150] F.A. Harrison, F.E. Christensen, W. Craig, C. Hailey, W. Baumgartner, C.M.H. Chen, J. Chonko, W. Rick Cook, J. Collin, K.-K. Madsen, M. Pivavoroff,

S. Boggs, D. Smith. Exp. Astron., **20** (1), 131 (2005). DOI: 10.1007/s10686-006-9072-z
[151] W.W. Zhang. Proc. SPIE, **7437**, 74370N (2009). DOI: 10.1117/12.830225
[152] J.E. Koglin, H.J. An, K.L. Blaedel, N. Brejnholt, F.E. Christensen, W.Craig, T.A. Decker, C.J. Hailey, L.C. Hale, F.A. Harrison, C.P. Cooper-Jensen, K.K. Madsen, K. Mori, M.J. Pivovaroff, G. Tajiri, W.W. Zhang. Proc. SPIE, **7437**, 74370C (2009). DOI: 10.1117/12.826724
[153] F.A. Harrison, S. Boggs, F.E. Christensen, W. Craig, C. Hailey, D. Stern, W. Zhang, L. Angelini, H.-J. An, V. Bhalereo, N. Brejnholt, L. Cominsky, W. Rick Cook, M. Doll, P. Giommi, B. Grefenstette, A. Hornstrup, V.M. Kaspi, Y. Kim, T. Kitaguchi, J. Koglin, C.C. Liebe, G. Madejski, K.K. Madsen, P. Mao, D. Meier, H. Miyasaka, K. Mori, M. Perri, M. Pivovaroff, S. Puccetti, V. Rana, A. Zoglauer. Proc. SPIE, **7732**, 7732OS (2010). DOI: 10.1117/12.858065
[154] W.W. Craig, H. An, K.L. Blaedel, F.E. Christensen, T.A. Decker, A. Fabricant, J. Gum, C.J. Hailey, L. Hale, C.B. Jensen, J.E. Koglin, K. Mori, M. Nynka, M.J. Pivovaroff, M.V. Sharpe, M. Stern, G. Tajiri, W.W. Zhang. Proc. SPIE, **8147**, 81470H (2011). DOI: 10.1117/12.895278
[155] F.E. Christensen, A.C. Jakobsen, N.F. Brejnholt, K.K. Madsen, A. Hornstrup, N.J. Westergaard, J. Momberg, J. Koglin, A.M. Fabricant, M. Stern, W.W. Craig, M.J. Pivovaroff, D. Windt. Proc. SPIE, **8147**, 81470U (2011). DOI: 10.1117/12.894615
[156] F.A. Harrison, W.W. Craig, F.E. Christensen, C.J. Hailey, W.W. Zhang, S.E. Boggs, D. Stern, W. Rick Cook, K. Forster, P. Giommi, B.W. Grefenstette, Y. Kim, T. Kitaguchi, J.E. Koglin, K.K. Madsen, P.H. Mao, H. Miyasaka, K. Mori, M. Perri, M.J. Pivovaroff, S. Puccetti, V.R. Rana, N.J. Westergaard, J. Willis, A. Zoglauer, H. An, M. Bachetti, N.M. Barriffere, E.C. Bellm, V. Bhalerao, N.F. Brejnholt, F. Fuerst, C.C. Liebe, C.B. Markwardt, M. Nynka, J.K. Vogel, D.J. Walton, D.R. Wik, D.M. Alexander, L.R. Cominsky, A.E. Hornschemeier, A. Hornstrup, V.M. Kaspi, G.M. Madejski, G. Matt, S. Molendi, D.M. Smith, J.A. Tomsick, M. Ajello, D.R. Ballantyne, M. Balokovic, D. Barret, F.E. Bauer, R.D. Blandford, W. Niel Brandt, L.W. Brenneman, J. Chiang, D. Chakrabarty, J. Chenevez, A. Comastri, F. Dufour, M. Elvis, A.C. Fabian, D. Farrah, C.L. Fryer, E.V. Gotthelf, J.E. Grindlay, D.J. Helfand, R. Krivonos, D.L. Meier, J.M. Miller, L. Natalucci, P. Ogle, E.O. Ofek, A. Ptak, S.P. Reynolds, J.R. Rigby, G. Tagliaferri, S.E. Thorsett, E. Treister, C.M. Urry. Astrophys. J., **770** (103), 103 (2013). DOI: 10.1088/0004-637X/770/2/103
[157] K. Forster, F.A. Harrison, S.R. Dodd, D.K. Stern, H. Miyasaka, K.K. Madsen, B.W. Grefenstette, C.B. Markwardt, W.W. Craig, F.E. Marshall. Proc. SPIE, **9149**, 91490R (2014). DOI: 10.1117/12.2056916
[158] K.K. Madsen, F.E. Christensen, W.W. Craig, K.W. Forster, B.W. Grefenstette, F.A. Harrison, H. Miyasaka, V. Rana. J. Astron. Telesc. Instrum. Syst., **3** (4), 044003 (2017). DOI: 10.1117/1.JATIS.3.4.044003
[159] M. Ghigo, S. Basso, R. Canestrari, L. Proserpio. Proc. SPIE, **7439**, 74390M (2009). DOI: 10.1117/12.826405
[160] B. Salmaso, S. Basso, C. Brizzolari, M. Civitani, M. Ghigo, G. Pareschi, D. Spiga, G. Tagliaferri, G. Vecchi. Proc. SPIE, **9151**, 91512W (2014). DOI: 10.1117/12.2056038
[161] V. Navalkar, K.P. Singh, M. Press. J. Astrophys. Astron., **40** (3), 24 (2019). DOI: 10.1007/s12036-019-9592-3
[162] F. Kislat, B. Beheshtipour, P. Dowkontt, V. Guarinoy, R.J. Lanzi, T. Okajima, D. Braun, S. Cannon, G. De Geronimo, S. Heatwole, J. Hoorman, S. Li, H. Mori, C.M. Shreves, D. Stuchlik, H. Krawczynski. J. Astron. Instrum., **6** (2), 1740003 (2017). DOI: 10.1142/S2251171717400037
[163] H. Awaki, H. Kunieda, M. Ishida, H. Matsumoto, Y. Babazaki, T. Demoto, A. Furuzawa, Y. Haba, T. Hayashi, R. Iizuka, K. Ishibashi, N. Ishida, M. Itoh, T. Iwase, T. Kosaka, D. Kurihara, Y. Kuroda, Y. Maeda, Y. Meshino, I. Mitsuishi, Y. Miyata, T. Miyazawa, H. Mori, H. Nagano, Y. Namba, Y. Ogasaka, K. Ogi, T. Okajima, S. Saji, F. Shimasaki, T. Sato, T. Sato, S. Sugita, Y. Suzuki, K. Tachibana, S. Tachibana, S. Takizawa, K. Tamura, Y. Tawara, T. Torii, K. Uesugi, K. Yamashita, S. Yamauchi. Appl. Opt., **53** (32), 7664 (2014). DOI: 10.1364/AO.53.007664
[164] K. Tamura, H. Kunieda, Y. Miyata, T. Okajima, T. Miyazawa, A. Furuzawa, H. Awaki, Y. Haba, K. Ishibashi, M. Ishida, Y. Maeda, H. Mori, Y. Tawara, S. Yamauchi, K. Uesugi, Y. Suzuki, HXT Team. J. Astron. Telesc. Instrum. Syst., **4** (1), 011209 (2018). DOI: 10.1117/1.JATIS.4.1.011209
[165] H. Matsumoto, H. Awaki, M. Ishida, A. Furuzawa, S. Yamauchi, Y. Maeda, I. Mitsuishi, Y. Haba, T. Hayashi, R. Iizuka, K. Ishibashi, M. Itoh, H. Kunieda, T. Miyazawa, H. Mori, T. Okajima, S. Sugita, K. Tamura, Y. Tawara. J. Astron. Telesc. Instrum. Syst., **4** (1), 011212 (2018). DOI: 10.1117/1.jatis.4.1.011212
[166] K.K. Madsen, F. Harrison, D. Broadway, F.E. Christensen, M. Descalle, D. Ferreira, B. Grefenstette, D. Gurgew, A. Hornschemeier, H. Miyasaka, T. Okajima, S. Pike, M. Pivovaroff, T. Saha, D. Stern, J. Vogel, D. Windt, W. Zhang. Proc. SPIE, **10699**, 106996M (2018). DOI: 10.1117/12.2314117
[167] K. Madsen, R. Hickox, M. Bachetti, D. Stern, N.C. Gellert, J. García, E. Kara, N.W. Brandt, H. Krawczynski, A. Lohfink, L. Brenneman, F. Christensen, M. Middleton, A. Hornstrup, G. Matt, A. Jaodand, G. Lansbury, C. Ricci, F. Fuerst, D. Ballantyne, D. Walton, A. Fabian, D. Ferreira, K. Pottschmidt, J.M. Miller, D.L. Windt, M. Baloković, N. Kamraj, J. Wilms, M. Heida, D. Alexander, P. Boorman, D. Wik, J. Vogel, H. Earnshaw, M.-A. Descalle, F. Civano, F. Fornasini, J. Grindlay, W. Zhang, A. Hornschemeier, W. Craig. BAAS, **51** (7), 166 (2019).
[168] W.W. Zhang, K.D. Allgood, M.P. Biskach, K.-W. Chang, M. Hlinka, J.D. Kearney, J.R. Mazzarella, R.S. Mc Clelland, A. Numata, L.G. Olsen, R.E. Riveros, T.T. Saha, P.M. Solly. Proc. SPIE, **10399**, 103990S (2017). DOI: 10.1117/12.2270861
[169] M.J. Ciešlak, K.A. Gamage, R. Glover. Radiat. Meas., **92**, 59 (2016). DOI: 10.1016/j.radmeas.2016.08.002
[170] J. Knödlseder. Exp. Astron., **20** (1), 3 (2005). DOI: 10.1007/s10686-006- 9031-8
[171] H. Halloin, P. Bastie. Exp. Astron., **20** (1–3), 151 (2005). DOI: 10.1007/978- 1-4020-5304-7_17
[172] H. Halloin. Exp. Astron., **20** (1–3), 171 (2005). DOI: 10.1007/978-1-4020- 5304-7_18
[173] F. Frontera, P. von Ballmoos. X-ray Opt. Instrum., **2010** (1), ID 215375 (2010). DOI: 10.1155/2010/215375
[174] R.K. Smither. Rev. Sci. Instrum., **85**, (8), 081101 (2014). DOI: 10.1063/1.4893585.
[175] F. Frontera, G. Loffredo, A. Pisa, F. Nobili, V. Carassiti, F. Evangelisti, L. Landia, S. Squerzanti, E. Caroli,

J.B. Stephen, K.H. Andersen, P. Courtois, N. Auricchio, L. Milani, B. Negri. Proc. SPIE, **7011**, 70111R (2008). DOI: 10.1117/12.790484

[176] P. von Ballmoos, H. Halloin, J. Evrard, G. Skinner, N. Abrosimov, J. Alvarez, P. Bas tie, B. Hamelin, M. Hernanz, P. Jean, J. Knödlseder, B. Smither. Exp. Astron., **20** (1–3), 253 (2005). DOI: 10.1007/s10686-006-9071-0

[177] A. Pisa, F. Frontera, P. De Chiara, G. Loffredo, D. Pellicciotta, G. Landini, T. Franceschini, S. Silvestri, K. Andersen, P. Courtois, B. Hamelin. Proc. SPIE, **5536**, 39 (2004). DOI: 10.1117/12.563052

[178] F. Frontera, A. Pisa, G. Loffredo, D. Pellicciotta, V. Carassiti, F. Evangelisti, K. Andersen, P. Courtois, L. Amati, E. Caroli, T. Franceschini, G. Landini, S. Silvestri, J. Stephen. Exp. Astron., **20** (1–3), 241 (2005). DOI: 10.1007/s10686-006-9050-5

[179] D. Pellicciotta, F. Frontera, G. Loffredo, A. Pisa, K. Andersen, P. Courtois, B. Hamelin, V. Carassiti, M. Melchiorri, S. Squerzanti. IEEE Trans. Nucl. Sci., **53** (1), 253 (2006). DOI: 10.1109/TNS.2006.869823

[180] N. Barriére, P. von Ballmoos, P. Bastie, P. Courtois, N.V. Abrosimov, K. Andersen, T. Buslaps, T. Camus, H. Halloin, M. Jentschel, J. Knödlseder, G. Roudil, D. Serre, G. Skinner. Proc. SPIE, **6688**, 66880O (2007). DOI: 10.1117/12.733993

[181] J. Knödlseder, P. von Ballmoos, F. Frontera, A. Bazzano, F. Christensen, M. Hernanz, C. Wunderer. Exp. Astron., **23** (1), 121 (2009). DOI: 10.1007/s10686-008-9119-4

[182] P. von Ballmoos, H. Halloin, G. Skinner, R.K. Smither, J. Paul, N.V. Abrosimov, J.M. Alvarez, P. Astier, P. Bastie, D. Barret, A. Bazzano, A. Boutonnet, P. Brousse, B. Cordier, T. Courvoisier, G. Di Cocco, A. Giuliani, B. Hamelin, M. Hernanz, P. Jean, J. Isern, J. Knödlseder, P. Laurent, F. Lebrun, A. Marcowith, V. Martinot, L. Natalucci, J.-F. Olive, R. Pain, R. Sadat, H. Sainct, P. Ubertini, G. Vedrenne. Proc. SPIE, **5168**, 482 (2004). DOI: 10.1117/12.509672

[183] N. Barriére, P. von Ballmoos, H. Halloin, N. Abrosimov, J.M. Alvarez, K. Andersen, P. Bastie, S. Boggs, P. Courtois, T. Courvoisier, M. Harris, M. Hernanz, J. Isern, P. Jean, J. Knödlseder, G. Skinner, B. Smither, P. Ubertini, G. Vedrenne, G. Weidenspointner, C. Wunderer. Exp. Astron., **20** (1), 269 (2005). DOI: 10.1007/978-1-4020-5304-7_27

[184] P. von Ballmoos, J. Alvarez, N. Barriere, S. Boggs, A. Bykov, J.M. Del Cura Velayos, F. Frontera, L. Hanlon, M. Hernanz, E. Hinglais, J. Isern, P. Jean, J. Knödlseder, L. Kuiper, M. Leising, B. Pirard, J.-P. Prost, R. da Silva, T. Takahashi, J. Tomsick, R. Walter, A. Zoglauer. Proc. SPIE, **8145**, 81450E (2011). DOI: 10.1117/12.895419

[185] F. Frontera, E. Virgilli, V. Carassiti, C. Guidorzi, P. Rosati, L. Amati, N. Auricchio, L. Bassani, R. Campana, E. Caroli, F. Fuschino, R. Gilli, C. Labanti, A. Malizia, M. Orlandini, J.B. Stephen, G. Stratta, S. Del Sordo, G. Ghirland, S. Brandt. Mem. S.A.It., **90**, 247 (2019).

[186] N. Barriére, J. Rousselle, P. von Ballmoos, N.V. Abrosimov, P. Courtois, P. Bastie, T. Camus, M. Jentschel, V.N. Kurlov, L. Natalucci, G. Roudil, N.F. Brejnholtg, D. Serreh. J. Appl. Cryst., **42** (5), 834 (2009). DOI: 10.1107/S0021889809023218

[187] W.H. Zahariasen. Acta Cryst., **23**, 558 (1967). DOI: 10.1107/S0365110X67003202

[188] N. Lund. Exp. Astron., **20** (1–3), 211 (2005). DOI: 10.1007/s10686-006-9026-5

[189] R.K. Smither, K.A. Saleem, D.E. Roa, M.A. Beno, P. Von Ballmoos, G.K. Skinner. Exp. Astron., **20** (1), 201 (2005). DOI: 10.1007/s10686-005-9019-9

[190] P. Courtois, T. Bigault, K.H. Andersen, J. Baudin-Cavallo, K. Ben Saïdane, M. Berneron, A. El-Aazzouzzi, D. Gorny, W. Graf, T. Guiblain, R. Hehn, E. Hetzler, C. Menthonnex, B. Mestrallet, C. Dewhurst. Physica B, 385–386, 1271 (2006). DOI: 10.1016/j.physb.2006.06.043

[191] S.F. Trevino, D.F.R. J. Mildner. Appl. Cryst., **37** (2), 339 (2004). DOI: 10.1107/S0021889804001785

[192] K. Nyilas, C. Dupas, T. Kruml, L. Zsoldos, T. Ungár, J.L. Martin. Mat. Sci. Eng. A, 387–389, 25 (2004).

[193] C. Ferrari, L. Zanotti, A. Zappettini, S. Arumainathan. Proc. SPIE, **7077**, 70770O (2008). DOI: 10.1117/12.796682

[194] R.K. Smither, P.B. Fernandez, T. Graber, P. von Ballmoos, J. Naya, F. Albernhe, G. Vedrenne, M. Faiz. Proc. SPIE, **2806**, 509 (1996). DOI: 10.1117/12.254001

[195] C. Malgrange. Cryst. Res. Technol., **37** (7), 654 (2002). DOI: 10.1002/1521-4079(200207)37:7¡654::AID-CRAT654¿3.0.CO;2-E

[196] E. Virgilli, V. Valsan, F. Frontera, E. Caroli, V. Liccardo, J.B. Stephen. J. Astrophys. Telesc. Instrum. Syst., **3**, 044001 (2017). DOI: 10.1117/1.JATIS.3.4.044001

[197] N. Barriére, V. Guidi, V. Bellucci, R. Camattari, T. Buslaps, J. Rousselle, G. Roudil, F.-X. Arnaud, P. Bastie, L. Natalucci. J. Appl. Cryst., **43** (6), 1519 (2010). DOI: 10.1107/S0021889810038343

[198] C. Ferrari, E. Buffagni, E. Bonnini, D. Korytar. J. Appl. Cryst., **46** (6), 1576 (2013). DOI: 10.1107/S0021889813022954

[199] E. Buffagni, C. Ferrari, F. Rossi, L. Marchini, A. Zappettini. Opt. Eng., **51** (5), 056501 (2012). DOI: 10.1117/12.893701

[200] V. Bellucci, R. Camattari, V. Guidi, I. Neri, N. Barriére. Exp. Astron., **31** (1), 45 (2011). DOI: 10.1007/s10686-011-9226-5

[201] V. Bellucci, R. Camattari, V. Guidi, A. Mazzolari. Thin Solid Films, **520** (3), 1069 (2011). DOI: 10.1016/j.tsf.2011.09.005

[202] R. Camattari, V. Guidi, L. Lanzoni, I. Neri. Meccanica, **48** (8), 1875 (2013). DOI: 10.1007/s11012-013-9734-7

[203] V. Bellucci, R. Camattari, V. Guidi, A. Mazzolari, G. Paterno, G. Mattei, C. Scian, L. Lanzoni. Appl. Phys. Lett., **107** (6), 064102 (2015). DOI: 10.1063/1.4928553

[204] R. Camattari, G. Paterno, M. Romagnoni, V. Bellucci, A. Mazzolari, V. Guidi. J. Appl. Cryst., **50** (1), 145 (2017). DOI: 10.1107/S1600576716018768

[205] R. Camattari, M. Romagnoni, A. Mazzolari, G. Paterno, V. Guidi, T. Buslaps. Exp. Astron., **46** (10), 309 (2018). DOI: 10.1007/s10686-018-9603-4

[206] R. Camattari, E. Dolcini, V. Bellucci, A. Mazzolari, V. Guidi. J. Appl. Cryst., **47** (5), 1762 (2014). DOI: 10.1107/S1600576714018834

[207] A. Erko, F. Schafers, W. Gudat, N.V. Abrosimov, S.N. Rossolenko, V. Alex, S. Groth, W. Schröder. Nucl. Instrum. Methods Phys. Res. A, **374** (3), 408 (1996). DOI: 10.1016/0168-9002(96)00199-4

[208] N.V. Abrosimov. Exp. Astron., **20** (1), 185 (2005). DOI: 10.1007/978-1-4020-5304-7_19

[209] N.V. Abrosimov, S.N. Rossolenko, V. Alex, A. Gerhardt, W. Schröder. J. Crystal Growth, **166** (1–4), 657 (1996). DOI: 10.1016/0022-0248(96)00036-X

[210] S. Keitel, C. Malgrange, T. Niemoller, T. Schneider. Acta Crystallogr. A, **55** (5), 855 (1999). DOI: 10.1107/s010876739900313x
[211] R. Camattari, A. Battelli, V. Bellucci, V. Guidi. Exp. Astron., **37** (1), 1 (2014). DOI: 10.1007/s10686-013-9358-x
[212] O. Sumbaev. Soviet Phys. JETP, **5** (6), 1042 (1957).
[213] O.I. Sumbaev. Soviet Phys. JETP, **27**, 724 (1968).
[214] R. Camattari, V. Guidi, V. Bellucci, A. Mazzolari. J. Appl. Cryst., **48** (4), 977 (2015). DOI: 10.1107/S1600576715009875
[215] V. Guidi, V. Bellucci, R. Camattari, I. Neri. J. Appl. Cryst., **44** (6), 1255 (2011). DOI: 10.1107/S0021889811035709
[216] V. Bellucci, R. Camattari, V. Guidi. Astron. Astrophys. (A&A), **560**, A1 (2013). DOI: 10.1051/0004-6361/201322053
[217] R. Camattari, G. Paternó, V. Bellucci, V. Guidi. Exp. Astron., **38** (3), 417 (2014). DOI: 10.1007/s10686-014-9429-7
[218] R. Camattari, V. Guidi, V. Bellucci, I. Neri, F. Frontera, M. Jentschel. Rev. Sci. Instr., **84** (5), 053110 (2013). DOI: 10.1063/1.4807289
[219] R. Camattari, G. Paternó, A. Battelli, V. Bellucci, P. Bastie, V. Guidi. J. Appl. Cryst., **47** (2), 799 (2014). DOI: 10.1107/S1600576714005056
[220] R. Camattari, V. Guidi. Astron. Astrophys. (A&A), **570**, A17 (2014). DOI: 10.1051/0004-6361/201424463
[221] N.M. Barriére, L. Natalucci, N. Abrosimov, P. von Ballmoos, P. Bastie, P. Courtois, M. Jentschel, J. Knödlseder, J. Rousselle, P. Ubertini. Proc. SPIE, **7437**, 74370K (2009). DOI: 10.1117/12.826138
[222] N.M. Barriére, J.A. Tomsick, S.E. Boggs, A. Lowell, P. von Ballmoos. Proc. SPIE, **8147**, 81471D (2011). DOI: 10.1117/12.899893
[223] F. Frontera, G. Loffredo, A. Pisa, L. Milani, F. Nobili, N. Auricchio, V. Carassiti, F. Evangelisti, L. Landi, S. Squerzanti, K.H. Andersen, P. Courtois, L. Amati, E. Caroli, G. Landini, S. Silvestri, J.B. Stephen, J.M. Poulsen, B. Negri, G. Pareschi. Proc. SPIE, **6688**, 20 (2007). DOI: 10.1117/12.736038
[224] N. Barriére, P. von Ballmoos, L. Natalucci, G. Roudil, P. Bastie, P. Courtois, M. Jentschel, N.V. Abrosimov, J. Rousselle. Proc. SPIE, **10566**, 1056603 (2008). DOI: 10.1117/12.2308289
[225] E. Virgilli, F. Frontera, P. Rosati, V. Liccardo, S. Squerzanti, V. Carassiti, E. Caroli, N. Auricchio, J.B. Stephen. Pros. SPIE, **9603**, 960308 (2015). DOI: 10.1117/12.2190335
[226] C. Wade, N. Barriére, L. Hanlon, S.E. Boggs, N.F. Brejnholt, S. Massahi, J.A. Tomsick, P. von Ballmoos. Proc. SPIE, **9603**, 960309 (2015). DOI: 10.1117/12.2187029
[227] C. Wade, N.M. Barriére, J.A. Tomsick, L. Hanlon, S.E. Boggs, A. Lowell, P. von Ballmoos, S. Massahi. Nucl. Instr. and Meth. A, **895**, 135 (2018). DOI: 10.1016/j.nima.2018.04.005
[228] I. Mohacsi, P. Karvinen, I. Vartiainen, V.A. Guzenko, A. Somogyi, C.M. Kewish, P. Mercere, C. David. J. Synchrotron Radiat., **21** (3), 497 (2014). DOI: 10.1107/S1600577514003403
[229] G.K. Skinner. Astron. Astrophys., **383** (2), 352 (2002). DOI: 10.1051/0004-6361:20010745
[230] G.K. Skinner. Astron. Astrophys., **375** (1), 691 (2001). DOI: 10.1051/0004-6361:20011700
[231] G.K. Skinner. Appl. Optics, **43** (25), 4845 (2004). DOI: 10.1364/AO.43.004845
[232] P. Gorenstein. Proc. SPIE, **5168**, 411 (2004). DOI: 10.1117/12.506443
[233] P. Gorenstein, W. Cash, N. Gehrels, K. Gendreau, J. Krizmanic, M. Coleman Miller, C.S. Reynolds, R.M. Sambruna, G. Skinner, R.E. Streitmatter, D.L. Windt. Proc. SPIE, **7011**, 70110U (2008). DOI: 10.1117/12.789978
[234] G.K. Skinner. X-Ray Opt. Instrum., **2010** (4), ID 743485 (2010). DOI: 10.1155/2010/743485
[235] C. Braig, P. Predehl. Exp. Astron., **27** (3), 131 (2010). DOI: 10.1007/s10686- 009-9180-7
[236] C. Braig, P. Predehl. Opt. Eng., **51** (9), 096501 (2012). DOI: 10.1117/1.OE.51.9.096501
[237] C. Braig, I. Zizak. Appl. Opt., **57** (8), 1857 (2018). DOI: 10.1364/AO.57.001857
[238] C. Braig, P. Predehl. Appl. Opt., **46** (14), 2586 (2007). DOI: 10.1364/AO.46.002586
[239] B.R. Dennis, G.K. Skinner, M.J. Li, A.Y. Shih. Sol. Phys., **279** (2), 573 (2012). DOI: 10.1007/s11207-012-0016-7
[240] G.K. Skinner, Z. Arzoumaniana, W.C. Cash, N. Gehrels, K.C. Gendreauc, P. Gorenstein, J.F. Krizmanic, M.C. Miller, J.D. Phillips, R.D. Reasenberg, C.S. Reynolds, R.M. Sambruna, R.E. Streitmatter, D.L. Windt. Proc. SPIE, **7011**, 70110T (2008). DOI: 10.1117/12.789568
[241] C. Braig, P. Predehl. Exp. Astron., **21** (2), 101–123 (2006). DOI: 10.1007/s10686-006-9077-7
[242] C. Braig, P. Predehl. Proc. SPIE, **5488**, 601 (2004). DOI: 10.1117/12.551416
[243] M. Bavdaz, M.W. Beijersbergen, A.J. Peacock, R. Willingale, B. Aschenbach, H.W. Braeuninger. Proc. SPIE, **3766**, 94 (1999). DOI: 10.1117/12.363665
[244] J. Krizmanic, G. Skinner, N. Gehrels. Exp. Astron., **20** (1–3), 497 (2006). DOI: 10.1007/978-1-4020-5304-7_48